Additive Manufacturing and Characterization of Polyoxymethylene

by

Panxi Tian

A thesis submitted in partial fulfillment of the requirements for the degree of

Master of Science

Department of Mechanical Engineering
University of Alberta

Abstract

Fused deposition modeling (FDM) is one of the most commonly utilized additive manufacturing (AM) technologies around the world. It produces components via depositing materials layer by layer. Compared with traditional manufacturing methods, as well as other additive manufacturing techniques, FDM has received extensive attention because of its high degree of customization and low cost. In addition to the commonly utilized FDM materials, such as polylactic acid (PLA) and acrylonitrile butadiene styrene (ABS), a large number of new materials with unique properties became available for FDM technology in recent years .

Polyoxymethylene (POM) is an engineering thermoplastic that offers low friction and high impact resistance, and commonly used in many industrial applications, such as gear wheels and rifle stocks. It also has high stiffness, excellent wear resistance, and good chemical resistance, etc. However, POM is usually processed by traditional manufacturing methods, such as injection molding (IM) and extrusion. The potential of using POM for parts produced using FDM is extremely important both for industrial applications as well as for niche prototyping needs, but, so far, this has received very limited attention in the open literature.

The main motivation behind the current thesis is to close this aforementioned gap and to provide a first insight into the thermomechanical and elastic properties of in-house manufactured POM filaments and the use of them in our FDM machine. As such, the influence of infill direction on both elastic and viscoelastic properties, as well as the shear properties, of POM FDM parts were investigated.

The dimensional accuracy of FDM parts is the one of the key parameters to ensure that the dimensions of the manufactured parts match the design dimensions that leads to a successful production. ANOVA statistical analysis was applied to reveal the relationship between different printing conditions (i.e. the size

of the parts and the printing temperature) and the dimensional accuracy. In addition, industrial components are usually of different shapes, so the comparison of dimensional accuracy of different shapes was also studied in this thesis.

Keyword: fused deposition modelling, polyoxymethylene, extrusion, infill direction, elasticity and viscoelasticity, dimensional accuracy

Preface

This thesis is an original work by ‘Panxi Tian’. No part of this thesis has been previously published.

Acknowledgements

It is a wonderful but challenging experience throughout my life that gave me a whole new perspective to re-understand the world. I appreciate living and studying in such a warm and relaxed environment, surrounded by many nice people. Without their help, much of the work in this thesis would not be completed.

My sincerest thanks are to my supervisor and mentor, Dr. Cagri Ayranci for his encouragement and guidance in the past two years. His responsibility, seriousness, and patience has thought and guided me in this journey.

I would like to thank my girlfriend, Yunyi Ye for her support, accompany and sacrifice over the past two years. Whenever I feel confused, her words always make me regain confidence and overcome difficulties.

I would like to thank my family for their continuous support that has been shown to me in the last two years. Thank you for providing me with a good educational environment and unlimited care.

Last but not least, I am so happy to be with you: Yu Chen, Eyup Can Demir, and Irina Grace have spent an unforgettable two years together.

Contents

Chapter 1 Introduction **1**

1.1 Motivation 1

1.2 Thesis Objectives 1

1.3 Thesis Outline 3

Chapter 2 Background **4**

2.1 Additive Manufacturing 4

2.1.1 Background and History of Additive Manufacturing 4
2.1.2 Fused Deposition Modeling Process and Applications 6
2.1.3 Fused Deposition Modeling Parameters 10

2.2 Polyoxymethylene 12

2.2.1 Brief History of POM 12
2.2.2 Properties and Applications of POM 12

Chapter 3 Production and characterization of properties of POM filament **15**

3.1 Extrusion Process 16

3.2 Thermogravimetric Analysis and Differential Scanning Calorimetry Analysis 18

3.3 Mechanical Tests 21

Chapter 4 Characterization of Fused Deposition Modeling Parts Fabricated from POM **24**

4.1 Introduction 24

4.2 Methodology 25

4.2.1 Materials 25
4.2.2 Build Plate Adhesive Preparation 25
4.2.3 Fused Deposition Modeling 25
4.2.4 Tensile Test 28
4.2.5 Dynamic Mechanical Analysis 28
4.2.6 Torsion Test 29

4.3 Results and Discussion 31

4.3.1 Effect of infill direction on Elastic Properties 31
4.3.2 Effect of infill direction on Viscoelastic Properties 35
4.3.3 Shear Properties 39
4.4 Conclusions 40

Chapter 5 Analysis of the factors affecting the dimensional accuracy of POM FDM parts 42

5.1 Introduction 42
5.2 Methodology 43
5.2.1 Materials 43
5.2.2 Design of Experiments 43
5.2.3 Specimen Fabrication via FDM Method 44
5.2.4 Measurement 45
5.3 Results and Discussion 46
5.3.1 ANOVA Analysis 48
5.3.2 Main Effects 50
5.3.3 Interaction 51
5.3.4 Regression Models for Relative Error 52
5.3.5 Difference in dimensional accuracy between different shapes 54
5.4 Conclusions 55

Chapter 6 Summary and Future Works 57

6.1 Summary of the Thesis 57
6.2 Potential Future Work Recommendations 59

Bibliography 60

Appendix A 66

A.1 Staircase Effect 66
A.2 Containment Problem 66

Appendix B 67

List of Tables

Table 2.1 Significant FDM process parameters 10

Table 3.1 Process parameters for extrusion 17

Table 3.2 Selected speeds during the collection process 17

Table 3.3 Diameter of extruded POM filament in mm 18

Table 3.4 Summary of tensile testing results 22

Table 4.1 Typical properties of POM filament 25

Table 4.2 Process parameters for FDM 26

Table 4.3 Average elastic modulus (E) and standard deviation of different infill directions 32

Table 4.4 Average ultimate tensile strength (UTS) and standard deviation of different infill directions 33

Table 4.5 Average percent elongation at break ($EL\%$) and standard deviation of different infill directions 34

Table 4.6 Measurement of diameters and shear modulus of samples 40

Table 5.1 Thermal properties of POM filament 43

Table 5.2 Factors and their levels 44

Table 5.3 Design of Experiment for Triangle 46

Table 5.4 Design of Experiment for Square 47

Table 5.5 Design of Experiment for Hexagon 47

Table 5.6 Design of Experiment for Circle 48

Table 5.7 ANOVA table for Triangle..... 49

Table 5.8 ANOVA table for Square 49

Table 5.9 ANOVA table for Hexagon 49

Table 5.10 ANOVA table for Circle..... 49

Table 5.11 Regression analysis summary 53

List of Figures

Figure 2.1 Three different AM processes 5

Figure 2.2 Classification of different AM processes, adopted from [20] 6

Figure 2.3 FDM process chain 7

Figure 2.4 Two problems caused by 2.5D contours 8

Figure 2.5 Schematic diagram of FDM process 9

Figure 2.6 Five common infill patterns, adopted from [37] 11

Figure 2.7 POM homopolymers and copolymers 13

Figure 3.1 POM pellets used in the experiment 15

Figure 3.2 The schematic diagram of single screw extruder 16

Figure 3.3 Collection system 17

Figure 3.4 POM filament 18

Figure 3.5 TGA curve of POM filament 19

Figure 3.6 DSC curve of POM filament 20

Figure 3.7 Tensile testing of POM filament 21

Figure 3.8 Typical stress-strain curve of POM filament 22

Figure 4.1 The schematic diagram of tensile test sample based on ASTM D638-14 Type V in mm 27

Figure 4.2 Specimens with different infill directions for tensile testing 27

Figure 4.3 Experimental setup of tensile test 27
Figure 4.4 The schematic diagram of specimen for DMA test 29
Figure 4.5 The schematic diagram of the specimen for torsion test 30
Figure 4.6 MTS Torsion Master Testing System for torsion testing 30
Figure 4.7 Stress-strain curves of specimens with different infill directions 31
Figure 4.8 Comparison of elastic modulus for different infill directions 32
Figure 4.9 Comparison of ultimate tensile strength for different infill directions .. 33
Figure 4.10 Comparison of percent elongation at break for different infill directions 34
Figure 4.11 Comparison of storage modulus for different infill directions 36
Figure 4.12 Comparison of loss modulus for different infill directions 37
Figure 4.13 Comparison of loss tangent for different infill directions 38
Figure 4.14 Representative torque-angle of twist curve of POM FDM parts 40
Figure 5.1 Four different shape in two sizes with dimensions in mm 45
Figure 5.2 Actual FDM samples in two sizes on PLA plates 45
Figure 5.3 Main Effects Plot for Relative Error 50
Figure 5.4 Delamination between layers for Triangle and Square 51
Figure 5.5 Interaction Plot for Relative Plot 52
Figure 5.6 Interval Plot for Relative Error 55

Abbreviations

T_g	Glass Transition Temperature
T_m	Melting Temperature
X_c	Degree of Crystallinity
E	Elastic Modulus
UTS	Ultimate Tensile Strength
$EL\%$	Percent Elongation at Break
SD	Standard Deviation
G'	Storage Modulus
G''	Loss Modulus
$\tan \delta$	Loss Tangent
$Temp$	Temperature
G	Shear Modulus

Glossary of Terms

FDM	Fused Deposition Modeling
3DP	Three-dimensional Printing
AM	Additive Manufacturing
IM	Injection Molding
POM	Polyoxymethylene
HME	Hot Melt Extrusion
CM	Compression Molding
CAD	Computer-aided Design
SLA	Stereolithography
LOM	Laminated Objective Manufacturing
SLS	Selective Laser Sintering

RP	Rapid Prototyping
LM	Layered Manufacturing
ANOVA	Analysis of variance
FEA	Finite Element Analysis
MFR	Melt Flow Rate
TGA	Thermogravimetric Analysis
DSC	Differential Scanning Calorimetry
DMA	Dynamic Mechanical Analysis
DOE	Design of Experiments

Chapter 1 Introduction

1.1 Motivation

Fused deposition modeling (FDM), also known as three-dimensional printing (3DP) or Fused Filament Fabrication (FFF), is one of most commonly utilized additive manufacturing (AM) processes that is based on extrusion technology[1]. Due to its ability to produce customized products, it is widely used in medicine (bioprinting), art, manufacturing and engineering[2]. Compared to conventional fabrication processes, such as injection molding (IM), extrusion, and compression molding (CM), FDM provides a possibility to produce very complex components within a low cost and short time without the need for additional manufacturing techniques. Although FDM technology has been broadly used, the most commonly used printing thermoplastics materials are limited to PLA and ABS[3]. Other materials, such as Nylon, polytstyrene, polyethylene, have also started to be used in the last years, but the number of available polymers are still limited; therefore, it is necessary to explore more reliable and flexible printing materials for a wider range of applications[4].

1.2 Thesis Objectives

Polyoxymethylene (POM) is one of the thermoplastic materials that is widely used in industrial engineering applications where low friction and good wear characteristics is needed. It is used worldwide in automotive and electronic fields[5]. Additionally, it has excellent resistance to most organic solvents and chemicals[6]. Despite these attractive characteristics, POM has been used very little in literature for FDM. The use of POM in FDM would open great potentials for engineers and researchers in industry and academia that have a use for this material. This thesis was undertaken as a first attempt to close this gap.

During the study, first, extrusion is used to fabricate POM filaments. Process parameters have a dominant effect on the quality of final filament[7]. Thus, the

process parameters were carefully selected to manufacture the filament. Following the filament production, the analysis of mechanical and thermal properties of the POM filament was conducted. Later, POM filaments were used for the FDM process further to verify the feasibility of POM as new material and explore its characteristics. POM samples produced using FDM have been produced and mechanically and thermo-mechanically characterized. Finally, the influence of the size and the printing temperature on the dimensional accuracy of the has also been studied. The objectives of the present thesis are concluded as follows:

- Provide optimal extrusion parameters and a general understanding of the mechanical and thermal properties of POM filament.

- To extend the knowledge on the characteristics of POM FDM parts including elastic properties, viscoelastic properties and shear properties.

- Discuss the effect of the size and the printing temperature, and the influence of different shapes, on the dimensional accuracy of POM FDM parts. Provide useful suggestions for the design of industrial parts.

In addition, simple fitted models based on the current experiments are generated to predict the dimensional accuracy of POM FDM parts. Although the prediction is relatively rough, it can provide a design direction for POM FDM parts.

1.3 Thesis Outline

The current thesis is divided into six chapters. Chapter 2 provides insights into the fabrication technologies and the commonly used materials. Also reported in this chapter are topics related to the properties and applications of POM. In Chapter 3, the production process and the selected parameters during the extrusion of POM filament are described in detail. Experimental results and observations on the mechanical and thermal properties of POM filaments are reported in this chapter. The main focal point of Chapter 4 was to study the effect of infill direction on both elastic and viscoelastic properties of POM FDM parts. Also, a study was carried out to explore the shear properties of these materials. Chapter 5 illustrates the factors that affect the dimensional accuracy of POM FDM parts. This chapter provides suggestions for the production of POM industrial parts by FDM technology. The last chapter summarizes the findings and provides the direction for further research.

Chapter 2 Background

This chapter provides an overview of the history and related background of additive manufacturing (AM), with the main focus on Fused Deposition Modelling (FDM) and printing parameters. For the material (POM) that is used in this thesis, a brief introduction section is also presented that discusses its history, characteristic and applications. At last, recent researches respect to POM is mentioned to build up for Chapter 3.

2.1 Additive Manufacturing

2.1.1 Background and History of Additive Manufacturing

The start of additive manufacturing (AM) dates back to 1980s and began as a novel way of prototype manufacturing[8]. However, the concept of 3D printing (3DP) was firstly proposed by David E. H. Jones in 1974[9]. As its name implies, the process of 3D printing is similar to that of ordinary prints[10]. 3DP consists of 3 stages: first of all, the printing material enters the nozzle driven by the motor gear. Then, the material is melting in the nozzle via applying temperature, which exceeds its melting temperature (T_m). Finally, through the movement of the nozzle controlled by a computer, the melting material is placed on the build plate in a layer by layer manner. Unlike some conventional manufacturing techniques, 3DP does not need to prepare specific molds in advance to manufacture a product. It can create finished complex parts directly from computer aid design (CAD) models[11]. Because of its ease of use and rapid shaping ability, 3DP quickly became one of the popular manufacturing technologies[12], [13]. In 1984, Charles W. Hull applied Stereolithography (SLA) technology to produce a 3D object by in forming its cross-sectional pattern from a fluid medium as shown Figure 2.1(a)[14].

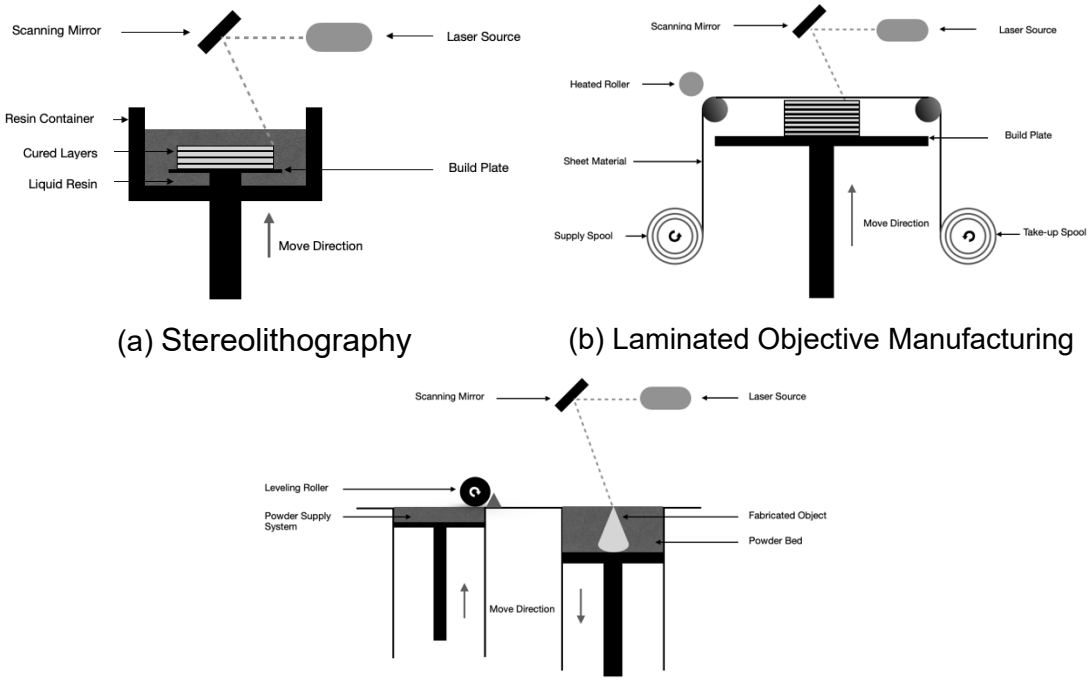

(a) Stereolithography (b) Laminated Objective Manufacturing

(c) Selective Laser Sintering

Figure 2.1 Three different AM processes

Three years later, Laminated object manufacturing (LOM) was invent by Michael Feygin, which is a process of forming a 3D object from laminations as shown in Figure 2.1(b)[15], [16]. In the same year, SLA as a kind of AM technologies was first used for commercial purposes[17]. Selective laser sintering (SLS) using a laser to selective sinter powder to form an object was introduced in 1989 as shown in Figure 2.1(c). Fused deposition modeling (FDM) is a 3D printing technique pioneered in 1989 by S. Scott Crump and his wife Lisa Crump, and Stratasys introduced the very first machine using this technology for industrial applications in 1992[18]. According to American Society for Testing and Materials (ASTM) International and The International Organization for Standardization (ISO), there are seven major categories of AM processes: Binder Jetting, Directed Energy Deposition, Material Extrusion, Material Jetting, Powder Bed Fusion, Sheet Lamination and Vat Photopolymerization[19]. Additionally, based on the states of raw material during the printing stage, AM technologies can be classified into three

categories: liquid, powder and solid states as Figure 2.2 shows. Although these technologies take a different approach, the principle of them is to add materials.

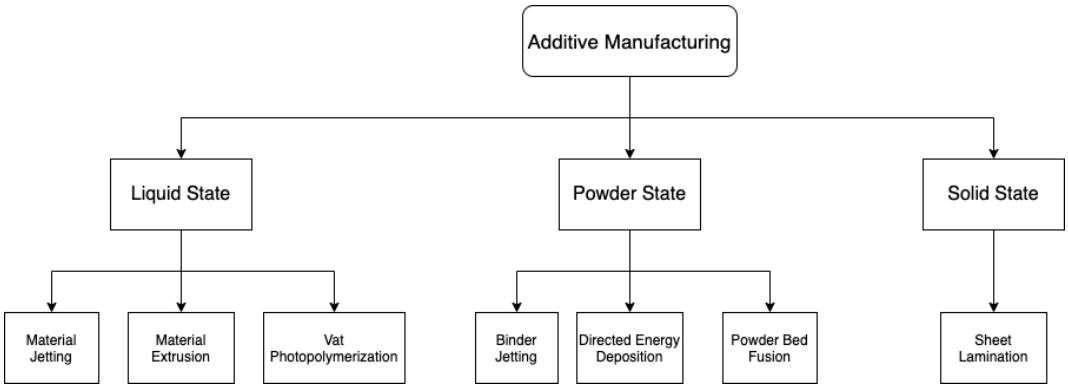

Figure 2.2 Classification of different AM processes, adopted from [20]

Among all AM processes, FDM is one of the fastest developing technology because of its low-cost and high-efficiency. In everyday life, FDM is often associated with commonly used 3D printers. Whether in the field of household or industrial manufacturing, with increasing demand for functional and cost-efficient products, many companies around the world have launched different 3D printers.

2.1.2 Fused Deposition Modeling Process and Applications

In general, Figure 2.3 shows that a typical FDM process that can be divided into four steps: modelling, slicing, programming and printing. In the modelling process, there are three ways to obtain 3D model: 1) Creating models 2) Downloading existing models 3) Scanning objects. Creating models is the most common method because it can produce different functional parts based on demands. Models are usually designed in CAD modeling software, such as AutoCAD and Solidworks. Generated CAD files are then exported as STL files, which is the standard file format in RP manufacturing and processed to slice[21].

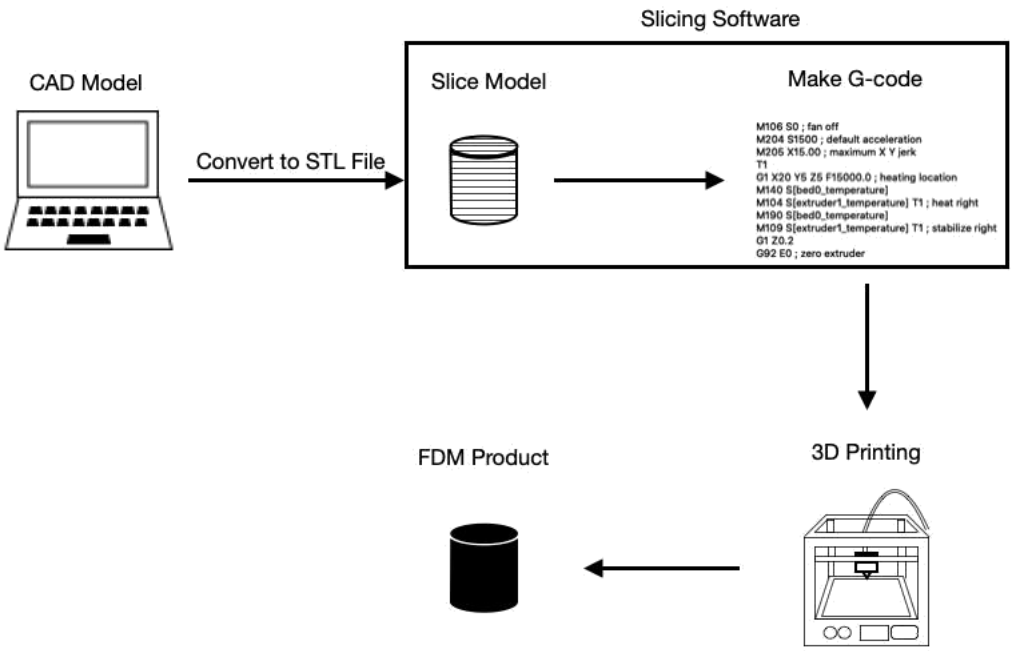

Figure 2.3 FDM process chain

Slicing the model is a crucial step for all layer manufacturing (LM) processes since it has an important impact on the accuracy and roughness of the final products. The slicing process is to segment the model into several uniform layers with a parallel horizontal plane in preparation for the layer stacking process[22]. However, the unidirectional slicing method slices layers into 2.5D contours which causes two problems[23]. The first one is the staircase effect, as Figure 2.4(a) shows, which loses the geometry of the surface along the vertical direction. Another problem raised to solve the staircase effect is the containment problem, Figure 2.4(b) shows toolpath could be inside or outside of the ideal geometry[24]. Many types of research have been done in an attempt to reduce these effects. Adaptive slicing is an effective method that determines the different layer thicknesses for slicing according to the shape of the model and printing performance[25]. In a word, the slicing process is the premise and basis of 3D printing.

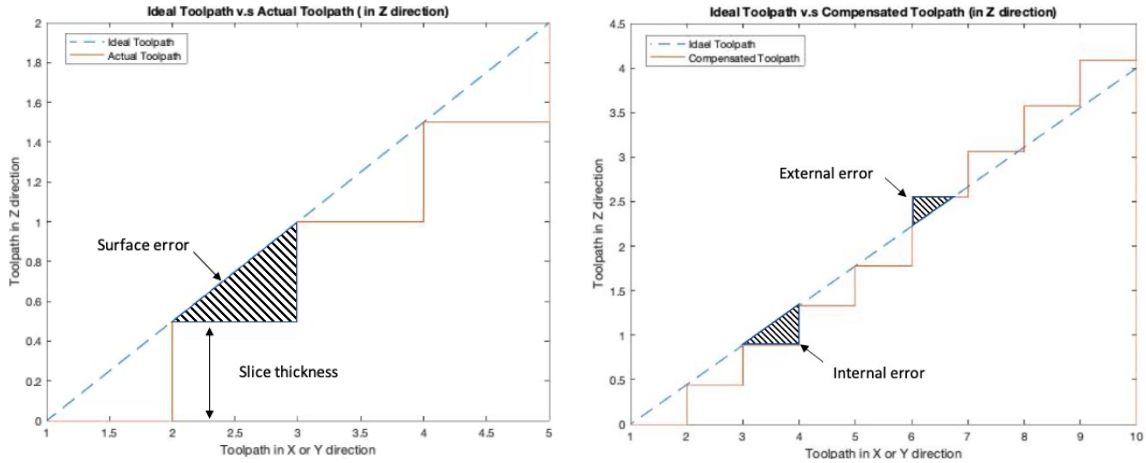

(a) Staircase Effect (b) Containment Problem

Figure 2.4 Two problems caused by 2.5D contours

G-code is generated based on the result of the slice, which is an industrial control language used to direct the movement of the machine. With the optimization and upgrade of different slicing software, slicing, parameter adjustment, and G-code generation have been integrated into one software. There are a number of slicing software (or called slicer) for 3D printers on the market, such as Cura, Simplify3D, Slic3r, and so on. All printing parameters and slicing processes can be done in these software, while most software also provides a visual printing simulation process.

The schematic diagram of FDM process is illustrated in Figure 2.5. The feedstock material in the form of flexible filament is fed into the print head assembly by a gear motor, and the material is partially melted. As the print head assembly moves, the semi-molten material is continuously extruded from the nozzle and stacked layer by layer on the build plate. The extruded layer solidifies at the room temperature and gets bonded with the neighboring one. Since the FDM system is based on this characteristic, the materials for FDM printing are limited to thermoplastics. The primary printing materials are ABS and PLA. Still, there are a number of other materials that have also attracted attention now, such as Nylon, Polycarbonates (PC), Polyethylene terephthalate (PET), and Thermoplastic polyurethane (TPU)[26]–[29]. Because of the excellent mechanical

properties of these materials, FDM technology has been widely used in households and industrial fields.

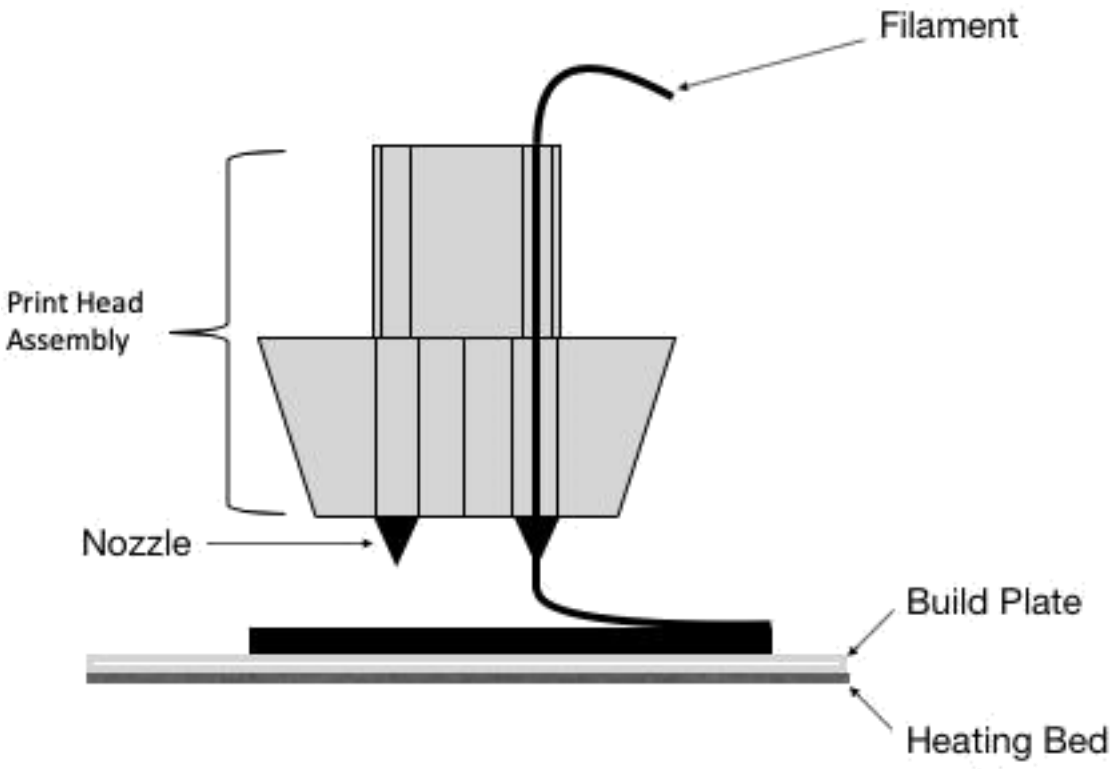

Figure 2.5 Schematic diagram of FDM process

Traditionally, FDM technology was used to produce prototypes due to limitations of materials and scale. However, with the innovation of technology, now FDM technology has also begun to emerge in many different new fields, such as aerospace, architecture, dentistry, and medical fields. In the past, prototypes of Unmanned Aerial Vehicle (UAV) components were often manufactured using FDM. Nowadays, because of its high cost-efficiency and high accuracy, it is often used to verify the structural efficiency of newly designed UAVs[30]. FDM is gradually applied in the construction field since this technology can fabricate any shape of house components in a short time without any waste[31]. With the aid of 3D scanning technology, it is proven that FDM is potent in producing temporary crowns and bridges, which can minimize the error of manual modeling[32]. By

setting specific parameters, FDM can be used to produce controlled drug delivery devices. Such devices are able to control the release rate of drugs, which is very important for treating diseases[33].

2.1.3 Fused Deposition Modeling Parameters

The mechanical properties of FDM parts highly depend on the FDM process parameters. Given the production process of FDM, in addition to room temperature and humidity, other parameters have a significant influence on the performance of the finished product, as Table 2.1 indicates.

Table 2.1 Significant FDM process parameters

Process parameters	**Common values**	**Description**
Printing Orientation	flat, on-edge, up-right	The direction of object building. Different printing directions show different mechanical performance.
Layer Height	0.2, 0.3, 0.4mm	The height of each layer. This value affects the resolution of parts.
Layer width	0.3, 0.45, 0.6mm	The width of each layer. This value is related to the width of the nozzle.
Wall Line Thickness	1.0 – 1.5mm[34]	The thickness of wall. This value affects the strength of the whole part.
Wall Line Counter	1, 2, 3	The number of walls. This value is equal to the ratio of wall line width and wall line thickness.
Infill Density	10 – 100%[35]	The density of infill material. This value strongly affects the strength of the part.
Printing Temperature*	180 – 240°C	The temperature during printing process. This value affects the state of the feedstock material and mechanical properties of the final part.
Build Plate Temperature*	40 – 80°C	The temperature set for the build plate. This value affects the adhesion and solidification speed of the layer.
Print Speed*	40 – 80mm/s[36]	The movement speed of the nozzle. This value determines the print time and partly affects the accuracy of the part.

* Value mainly depends on the properties of printing materials.

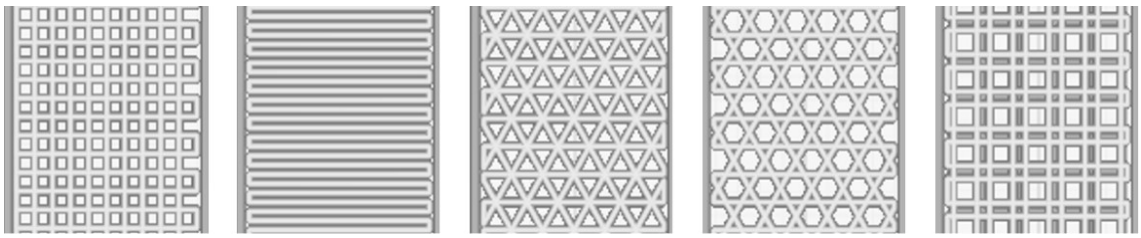

(a) Grid (b) Lines (c) Triangles (d) Hexagon (e) Octet

Figure 2.6 Five common infill patterns, adopted from [37]

Among all the process parameters, the quality and properties of the FDM part are greatly affected by the infill density, followed by the printing temperature[12]. The anisotropy of the part varies with the printing orientation while the infill direction is same[38]. Not only the resolution, but the surface roughness also depends on the layer height----the smaller the layer height, the lower the surface roughness[39]. The role of the wall line is to enhance the stiffness of the part; however, an increase in the number of wall lines will reduce the importance of infill performance[40]. In addition, although the infill pattern is not listed on the table, its impact on performance cannot be ignored[41]. Generally, the slicing software provides more than a dozen types of infill patterns for various purposes, but Figure 2.6 shows five of the most commonly used, namely, grid, lines, triangles, hexagon and octet. A detailed discussion about the influence of specific parameters will be included in Chapter 4.

The impacts of different factors and the effects of their interactions must be taken into account when selecting the appropriate parameters. Therefore, statistical analysis methods like Analysis of variance (ANOVA) and Taguchi method are useful tools to find the optimal parameter combination[42]. Furthermore, Finite Element Analysis (FEA), as simulation technology, gives a new perspective to analyze different parameter combinations, which is more intuitive and efficient[43].

2.2 Polyoxymethylene

2.2.1 Brief History of POM

Polyoxymethylene (POM) is also known as acetal or polyacetal, which is a semicrystalline engineering thermoplastic material. As a formaldehyde-based polymer, POM was firstly introduced by Aleksandr Butlerov in 1859 when he attempted to isolate methylene glycol[44]. Based on the properties of different polyoxymethylene, Auerbach and Barschall classified them according to their molecular structure into α-polyoxymethylene, β-polyoxymethylene, γ-polyoxymethylene and δ-polyoxymethylene, which is different from the current classification[45]. In 1926, Hermann Staudinger was devoted to deriving model systems suitable for more complex bio-polymers, so he started conducting in-depth research on single structural polymers such as formaldehyde and polystyrene[46]. POM was initially unsuitable for commercial use because of its thermal instability, but in 1952, researchers at DuPont found a chemical way to stabilize its basic molecule[47]. After eight years, DuPont produced the first commercial POM-H under the trademark Delrin®[48]. In the same year, Celanese Corporation, a specialty materials company from the United States, disclosed a process to manufacture POM-C and registered as a trademark Celcon® in 1962[49]. Subsequently, other manufacturers such as Ticona GmbH, Polyplastics and Ashai Kasei had also begun to produce different types of POM. Since POM has excellent properties, its market is experiencing a surge in demand from different industries in recent year.

2.2.2 Properties and Applications of POM

POM is a high molecule weight (up to 14200g/mol) thermoplastic polymer, which possesses high stiffness, low friction and excellent wear resistance[50]. The density of POM is between 1.4-1.6g/m^3, depending on the grade and manufacturer[51]. T_m and T_g of POM are usually around 170°C and -70°C, respectively[5]. Due to its high degree of crystallinity, POM is brittle at low

temperatures; but at the same time, it is one of the most fatigue resistant crystalline polymers[52]. POM has a relatively low water absorption rate which also means that it is insoluble in water and a lot of solvents near room temperature[53]. However, POM is sensitive to acids and oxidizing agents where it can degrade quickly[54].

In general, the production of POM-H and POM-C is the largest in the world among all types of POM and their chemical structures are shown in Figure 2.7. POM-H is synthesized by polymerizing anhydrous, monomeric formaldehyde while POM-C is synthesized by cationic copolymerization of comonomers. POM-H has better mechanical properties but is easy to depolymerize when heated. In contract, POM-C has better thermal stability but is poor in mechanical properties[5]. Given that, POM-C is more frequently used than POM-H.

(a) POM-H (b) POM-C

Figure 2.7 POM homopolymers and copolymers

As mentioned above, POM has excellent combination of properties making it widely used in various fields. Moreover, just like most thermoplastic materials, POM can be processed in many ways such as injection molding and extrusion[55]. In the automotive industry, POM is a good substitute for metals owing to its high dimensional stability and good sliding property. Due to its electrical and thermal insulation, POM is used to produce plugs, connectors and enclosures in electrical and electronic industry[56]. For medical uses, because POM possesses non-dissolving and inherent antibacterial properties, it is an excellent choice for

transporting pharmaceutical materials because of its non-dissolving and inherent antibacterial properties[57].

The application of FDM technology to the production of POM components will shorten prototype manufacturing time and provide a cost-effective material. Also, it will allow an excellent prototyping material for researchers and engineers. Therefore, it is worthwhile to study the feasibility of POM as FDM material. However, to date, research on the properties of POM FDM Parts is limited. This thesis will discuss the extrusion process of POM filament and the characteristics of POM FDM parts.

Chapter 3 Production and characterization of properties of POM filament

The POM used in this work is DURACON® M90-44 that was obtained from Polyplastics Co., Ltd, Japan. As Figure 3.1 illustrates, it is a copolymer in the granular (pellets) form with a density of 1.41g/m^3 and the melt flow rate (MFR) is 9g/10min. The recommended processing temperature for hot melt extrusion (HME) is between 190°C and 210°C[58].

Figure 3.1 POM pellets used in the experiment

The water absorption of this particular material is around 0.5% in 24h[58]. However, in order to minimize the impact of moisture, POM pellets were vacuum

dried in a Linderberg/Blue M^{TM} vacuum oven by maintaining temperature 85°C at 25MPa for 24h before the melt extrusion.

3.1 Extrusion Process

A single screw extruder (C.W. Brabender Laboratory Extruder MODEL 2503 and its length to diameter ratio (L/D) is 25:1) was used for the production of the filaments. As Figure 3.2 indicates, a single screw extruder consists of four major sections: (i) control panel, (ii) feed hopper, (iii) barrel, and (iv) die. Raw materials in the form of granules or powder are loaded into the feed hopper. By the movement of screws in the barrel, materials are transported through four heating zones, and melted materials are finally extruded through the die.

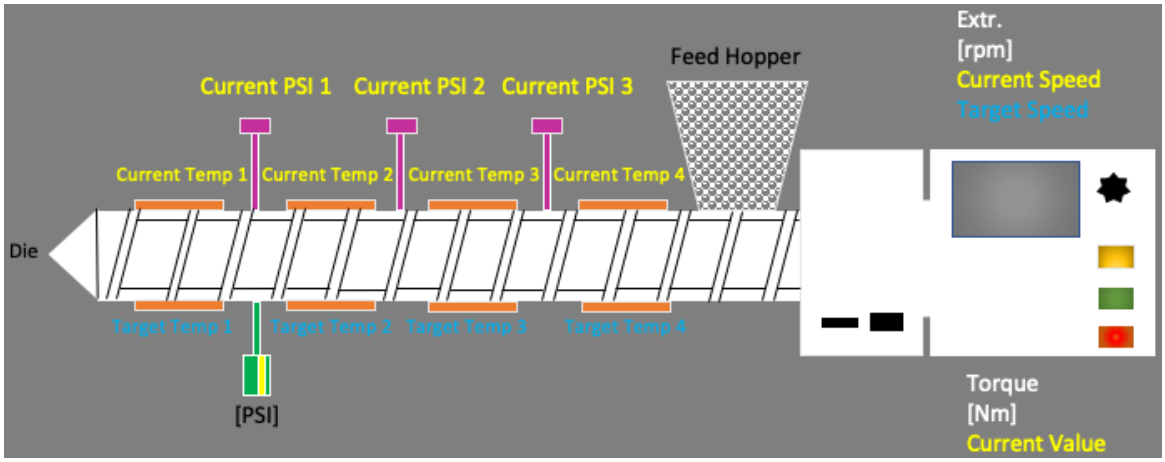

Figure 3.2 The schematic diagram of single screw extruder

At the beginning of the experiment, the parameters related to the extrusion process must be carefully considered, and the two main parameters are the screw speed and the barrel temperatures. The screw speed is related to the outlet pressure of the extruder and affects the quality of the filament. Barrel temperatures, including the temperature of all heating zones, mainly depend on the melting temperature (T_m) and MFR of the materials. Pure POM filament was obtained from a single screw extruder under the specific parameters, as Table 3.1 indicates.

Table 3.1 Process parameters for extrusion

Parameter	Unit	Value
Target Temp 1	°C	205
Target Temp 2	°C	205
Target Temp 3	°C	205
Target Temp 4	°C	160
Screw Speed	rpm	30
Torque	Nm	12.3

The collection system is composed of two parts shown in Figure 3.3: (a) conveyor, and (b) roller pulley. Once the material is extruded from the nozzle, it passes through the conveyor belt and is cooled and shaped by the two fans above the conveyor. The filament is then collected through a spool fixed on the pulley. The speeds selected in this experiment are shown in Table 3.2.

(a) Conveyor (b) Roller pulley

Figure 3.3 Collection system

Table 3.2 Selected speeds during the collection process

Component	Speed(rpm)
Conveyor Belt	28
Roller Pulley	20

A spool of collected POM filament is shown in Figure 3.4. The diameter of pure POM filaments was measure by a micrometer. Five positions were randomly selected on the filament for measurement.

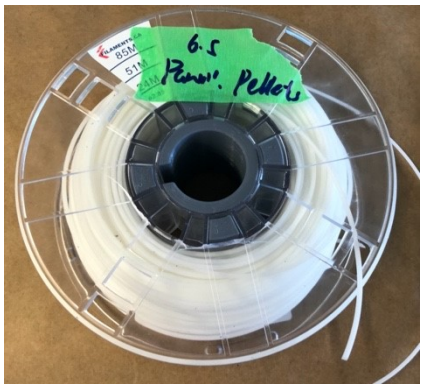

Figure 3.4 POM filament

Under the selected extrusion parameters, the diameter of the extruded filament samples and the standard deviation are listed in Table 3.3. It can be noted that the average diameter of them was about 2.7mm which was close to the standard diameter (2.85mm), while the standard deviation is 0.010 which implies that the diameter was stable enough. Therefore, it can be considered that the filament obtained under such conditions was suitable for the FDM process.

Table 3.3 Diameter of extruded POM filament in mm

Positions					Average	Standard Deviation
1	2	3	4	5		
2.742	2.756	2.768	2.746	2.749	2.752	0.010

3.2 Thermogravimetric Analysis and Differential Scanning Calorimetry Analysis

Thermogravimetric analysis (TGA) is a method of measuring the relationship between the mass of a substance and temperature or time under controlled temperature. By analyzing the TGA curve, the thermal stability and the thermal

decomposition of the sample can be known[59]. About 5mg sample was analyzed with TA Instruments Q50 Thermogravimetric Analyzer under nitrogen atmosphere in the range from 20°C to 600°C with a same ramp rate of 10°C/min.

Differential scanning calorimetry (DSC) is a thermoanalytical technique that can be applied to determine the thermal transitions of polymers[60]. DSC analysis was conducted to measure T_m of the pure POM. It was carried out under nitrogen atmosphere using TA Instrument DSC-Q1000. Approximately 10mg samples were cut from POM filament for the analysis.

The TGA curve of the POM filament is reported in Figure 3.5. The graph shows that the POM underwent thermal decomposition beginning at 252°C and 370°C was temperature when 50% of POM had decomposed. Moreover, the degradation of POM happened to be fast, which can be concluded from the slop of the curve. At 413°C, the POM was completely decomposed, leaving about 0.0104mg of impurities, accounting for about 0.3% of the total mass.

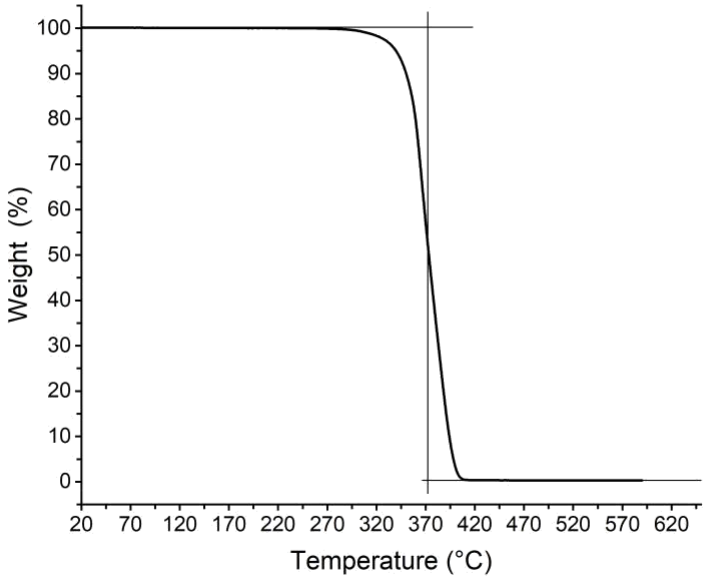

Figure 3.5 TGA curve of POM filament

Figure 3.6 displays the thermal behavior of POM filament via HME. It can be observed from the graph that the T_m of POM filament was around 165°C. A drop in the heat flow was found at 0°C, implying the glass transition temperature (T_g) of POM was lower than 0°C. As a result, POM usually behaviors like rubbery materials at room temperature, which was confirmed by Aoki *et al.*[61]. The degree of crystallinity (X_c) can be calculated by the following equation[62]:

$$X_c = \frac{H_m}{H_{f100}} \times 100\% \tag{3.1}$$

where H_m is the melting enthalpy determined from the peak area, and H_{f100} is the enthalpy of fusion of a 100% crystalline material (H_{f100} is approximately 273.1J/g for POM)[63]. It can be concluded that the X_c of POM was 49.7%.

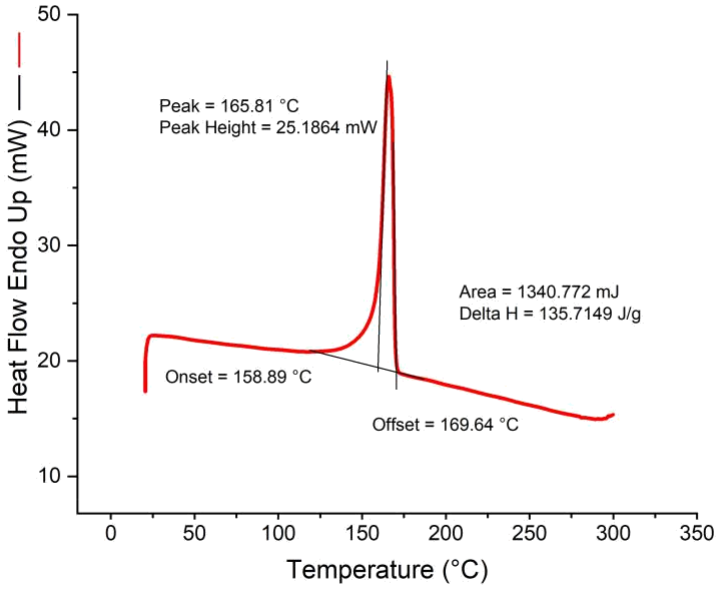

Figure 3.6 DSC curve of POM filament

3.3 Mechanical Tests

In order to investigate the mechanical properties of the POM filament, uniaxial tensile tests were carried out during this work (Figure 3.7). The ElectroForce® 3200 Series III test instruments fabricated by Bose corporation was applied for testing, which was furnished with a 450N load cell. The crosshead speed had been kept at 1mm/min at the room temperature (24°C) during the whole process, which can be regarded as quasi-static loading. The ends of tested filament samples were wrapped with parafilm to prevent the structure from being damaged or sliding during the tightening process.

Figure 3.7 Tensile testing of POM filament

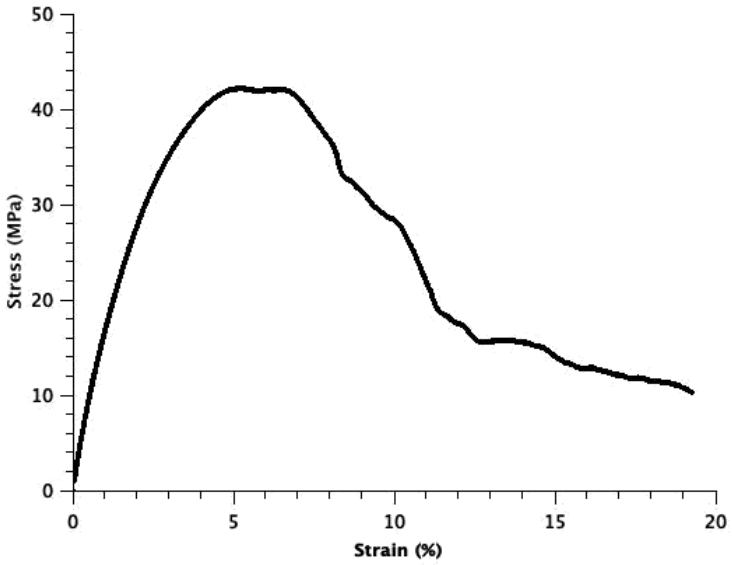

Figure 3.8 Typical stress-strain curve of POM filament

Table 3.4 Summary of tensile testing results

Material	Properties		
	Elastic Modulus (GPa)	Elongation at yield (%)	Ultimate Tensile Strength (MPa)
POM filament	1.27 ± 0.13	2.32 ± 0.07	42.15 ± 2.77

The typical stress-strain curve of POM filament has been presented in Figure 3.8. Table 3.4 outlines the summary of tensile properties of POM filament. It can be noticed that the elastic modulus was 1.27 ± 0.13GPa, the elongation at yield was 2.32 ± 0.07%, and the ultimate tensile strength was 42.15 ± 2.77MPa, which introduces the fundamental mechanical properties of POM filament. It must be noted that the filament started to pull out (slide-out) after the yield point. Therefore, the value of ultimate tensile strength may need to be checked with the use of different grips in the future.

Compare the results with that obtained from compression molding(CM), it can be found that the elastic modulus was around 960MPa, which is lower than the

extruded filament[64]. It is likely that more air bubbles could be introduced in the compression molding process, resulting in lower performance. However, the ultimate strength of the CM sample was reported at 55MPa, which is slightly larger than the extruded one[64]. The possible reasons for this difference could be as follows: 1) the condition of the tensile test is different, that is, the test speed is different, and it is easy to slip at high speed 2) the shape of the test sample is different, and it is easier for the filament to slip. The above two points could cause the ultimate tensile strength of the extruded filament smaller than that of the CM sample.

3.4 Conclusions

This chapter provides a general insight into the characteristics of POM filament. Specifically, TGA and DSC were carried out to detect the thermal properties of POM filament while the tensile test was conducted to investigate the mechanical properties of it. From the TGA results, it can be found that the temperature at which it began to decompose was around 252°C, indicating its poor thermal stability. According to the DSC graph, it shows the T_m of POM was about 165°C and the X_c of POM was 49.7%. Based on the tensile testing results, it reveals the basic mechanical properties of POM filament, i.e., the elastic modulus was 1.27 ± 0.13MPa, the elongation at yield was 2.32 ± 0.07% and the ultimate tensile strength was 42.15 ± 2.77MPa. The above properties are instructive for the further processing of POM filament. In future work, mixing POM with other materials and studying the properties of the mixtures will be a promising direction.

Chapter 4 Characterization of Fused Deposition Modeling Parts Fabricated from POM

4.1 Introduction

Polyoxymethylene (POM), also known as acetal or polyacetal, is a commonly used thermoplastic to engineer specific parts. Its superior properties, such as high strength (tensile strength is about 70MPa), low friction (0.280 and 0.139 for static and dynamic, respectively), and excellent wear resistance make it the best substitute for metals in many fields[65]–[67]. However, there is little research done in the literature on POM as an FDM material. Fraguas *et al.* focused on improving the adhesion of the build plate to improve the FDM POM parts[68]. Their work revealed the adhesive capacity of the build plate could be improved via treating it with atmospheric pressure air plasma. Wang studied the tensile properties of POM FDM parts, but their research was very limited and only included the maximum stress and strain in three unidirectional stacking directions, i.e., samples were printed at 0°, 45° and 90°[69]. Nevertheless, in the design stage, it requires more comprehensive performance characteristics as a reference to promoting POM FDM parts to meet functional requirements, none of these papers reported the DMA and torsional properties of POM FDM parts.

The present work focuses on three topics:

(i) Explore the elastic properties of POM FDM parts with different infill directions,

(ii) Investigate the viscoelastic properties of POM FDM parts with different infill directions, and

(iii) Study the shear properties of POM FDM parts.

4.2 Methodology

4.2.1 Materials

The main properties of POM filament (as presented in Section 3) are listed in Table 4.1. It was speculated that POM performs better under dry conditions[70]. Before further processing, the filament was dried at 85°C for 4h in order to minimize the impact of moisture absorption on the properties of the printed samples. ABS in the form pellets was purchased from Filabot used to prepare build plate adhesive.

Table 4.1 Typical properties of POM filament

Material	**Properties**		
	Elastic Modulus (GPa)	T_m (°C)	X_c (%)
POM	1.27	165	49.7

4.2.2 Build Plate Adhesive Preparation

The mixture of three different concentrations of ABS and acetone according to the amount of mixed ABS from small to large, called ABS juice, ABS glue, and ABS slurry, respectively. In this work, ABS glue was used as an adhesive between samples and the build plate. At first, 10g of ABS granules was added into 50ml of acetone and stored them in a closed glass container to prevent the evaporation of the solution. Then, a digital vortex mixer from Fisher Scientific was applied to dissolve ABS granules in solution fully. When the mixture appeared sticky, the ABS glue was complete.

4.2.3 Fused Deposition Modeling

When heated or mechanically abraded, POM may produce toxic formaldehyde gas, so it should be processed in a fume hood[71]. It is difficult to print POM-based samples because they do not adhere well to any typical 3D printer base surface. Therefore, ABS glue was used to improve the adhesive between them. In addition, the temperature difference between adjacent layers during printing could cause

the warpage of the sample. Thus, 3D printers with closed chambers are often used for printing POM material to slow down the temperature dissipation. It is also worth noting that a small layer thickness can reduce the impact of the warpage on performance[72].

In order to analyze the performance characteristics of POM FDM parts, three different specimens were designed in Solidworks. The CAD models of the specimens were then sliced in an open-source software named Cura and generated G-code for the 3D printer[37]. In the present study, the commercial 3D printer Ultimaker 3 was applied to fabricate samples. Many studies have shown that different process parameters affect the quality and performance of samples, Table 4.2 outlines the FDM processing parameters used during the experiments[73].

Table 4.2 Process parameters for FDM

Parameter	Unit	Value
Nozzle Diameter	mm	0.4
Build Orientation	-	Flat
Printing Temperature	°C	230
Build Plate Temperature	°C	60
Wall Line Count	-	1
Layer Height	mm	0.3
Layer Width	mm	0.35
Infill Density	%	100
Infill Pattern	-	Lines
Print Speed	mm/s	40

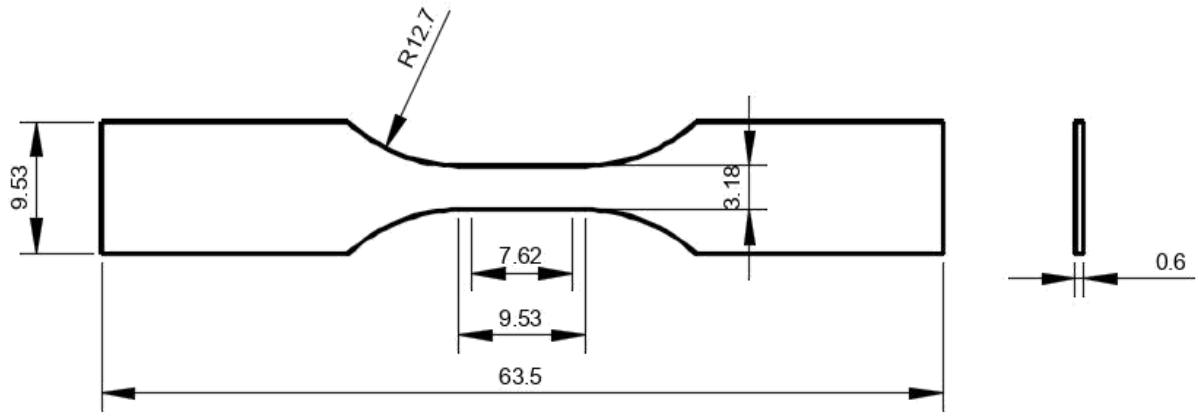

Figure 4.1 The schematic diagram of tensile test sample based on ASTM D638-14 Type V in mm

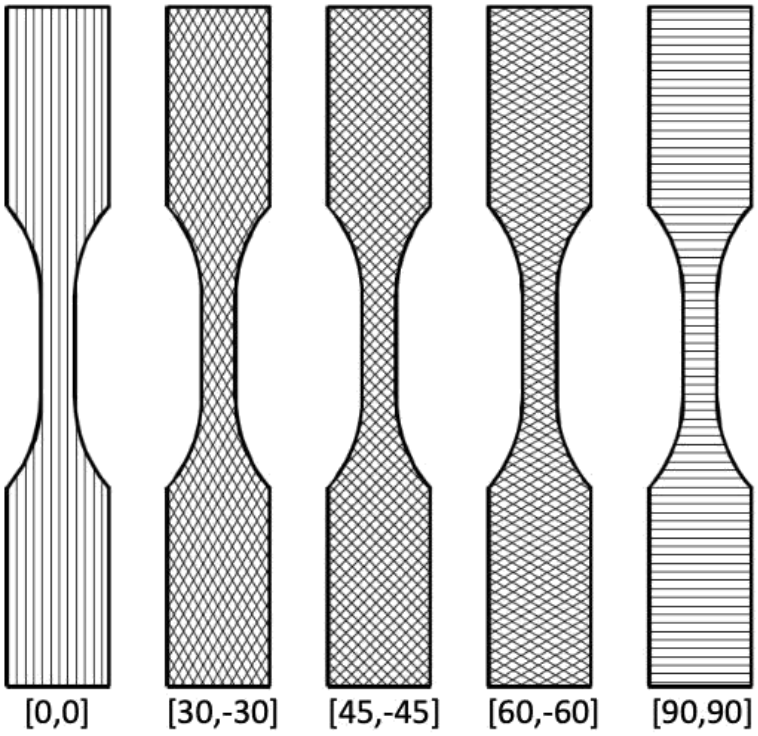

Figure 4.2 Specimens with different infill directions for tensile testing

Figure 4.3 Experimental setup of tensile test

4.2.4 Tensile Test

The uniaxial tensile tests were performed on ElectroForce® 3200 Series III test instruments, which was equipped with a 450N load cell. Since there are no standard specimens for the tensile tests of FDM parts, the geometry of sample used for printing in this experiment was based on ASTM D638-14 Type V as Figure 4.1 illustrates[74]–[76]. For the purpose of studying the influence of different infill direction on the mechanical performance, Figure 4.2 shows that five test specimens with different infill directions were fabricated. The specimens were printed at five different infill directions: [0,0], [30,-30], [45,-45], [60,-60] and [90,90]. 0° specimen has its toolpath along the longitudinal direction, while 90° specimen has its toolpath set 90° with respect to the longitudinal axis. The samples were tested at a rate of 1mm/min and the maximum crosshead displacement was 6.0mm. In order to ensure that the samples were tightened and not damaged, 11kN·mm torque was applied to tighten both upper and lower clamps as shown in Figure 4.3. All tests were conducted at room temperature (25°C) and the relative humidity of 24%. Under the given process parameters and environmental conditions, each set of samples was repeated five times, a total of 25 samples were used for testing.

4.2.5 Dynamic Mechanical Analysis

Dynamic mechanical analysis, abbreviated as DMA, is a technology for studying the viscoelastic behavior of polymers. When a sample is subjected to a stress or strain at controlled frequencies, the corresponding phase angle and deformation will be investigated[77]. To study the viscoelastic properties of the POM FDM parts, a rectangular specimen with 36mm × 12mm × 0.6mm from ASTM D5023-15 depicted in Figure 4.4 was designed for testing[78]. Similarly, five test specimens with different infill directions were produced for DMA. It was carried out to measure the storage modulus and loss modulus of POM FDM samples of different infill directions. DMA was performed on the TA Instruments Q800 Dynamic Mechanical Analyze at the heating rate of 10°C/min from -90°C to 130°C at 1Hz in nitrogen purge.

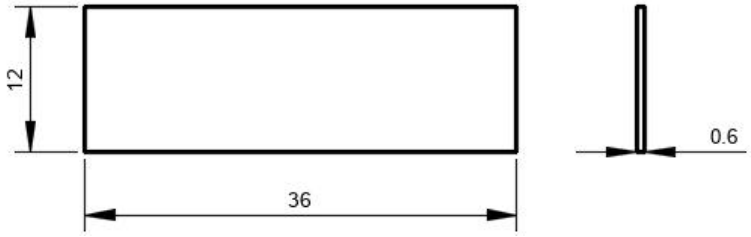

(a) Dimensions of the specimen for DMA test based on D5023-15 in mm

(b) FDM DMA sample

Figure 4.4 The schematic diagram of specimen for DMA test

4.2.6 Torsion Test

The aim of a torsion test is to determine the behavior of a material when twisted or under torsional force[79]. To study the shear properties of the POM FDM parts, as Figure 4.5 indicates, a hollow cylinder was fabricated with an outer diameter of 9mm and a wall thickness of 1mm according to ASTM E143-13[80]. A total of five samples produced from POM were tested and the gauge length of each specimen was 36 mm. The samples were secured in the torsion test device, an MTS Torsion Master Testing System (Model No.27.0000136) with a 20Nm load cell as Figure 4.6 illustrates. In order to tighten the grips without crushing the samples, metal plugs were firmly inserted into the ends. The hollow cylinder was tested under a constant angular rotation of $0.1 rads^{-1}$ and the transducer read the torque applied to it. All tests were conducted at an ambient temperature of 25°C. Data obtained at a rate of 10Hz from the experiment was plotted to reveal the relationship between torque and twist.

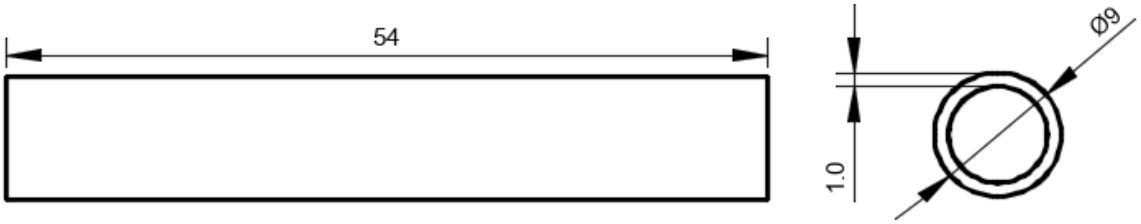

(a) Dimensions of the specimen for torsion test based on E143-13 in mm

(b) FDM hollow cylinder sample

Figure 4.5 The schematic diagram of the specimen for torsion test

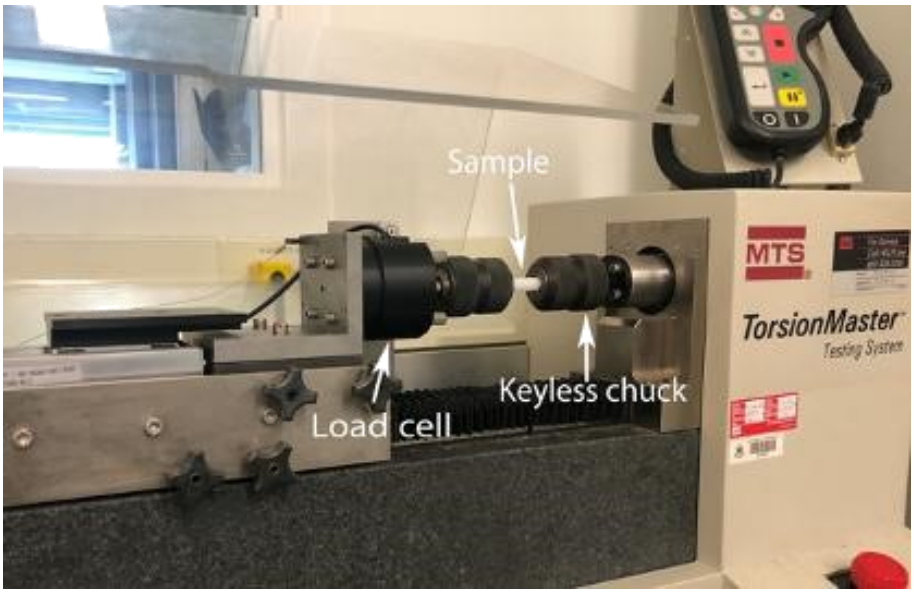

Figure 4.6 MTS Torsion Master Testing System for torsion testing

4.3 Results and Discussion

4.3.1 Effect of infill direction on Elastic Properties

The mechanical properties of POM FDM parts can be varied with different infill directions. Sood *et al.* confirmed that infill direction has a great impact on the tensile properties, and the proper infill direction could significantly improve the elastic features[81]. Figure 4.7 illustrates the representative stress-strain curves for FDM samples at [0,0], [30,-30], [45,-45], [60,-60] and [90,90], respectively. The typical curve selected from five samples of each infill direction clearly shows the anisotropy of the POM FDM parts. The three parameters investigated were the elastic modulus (E), the ultimate tensile strength (UTS), and the percent elongation at break ($El\%$).

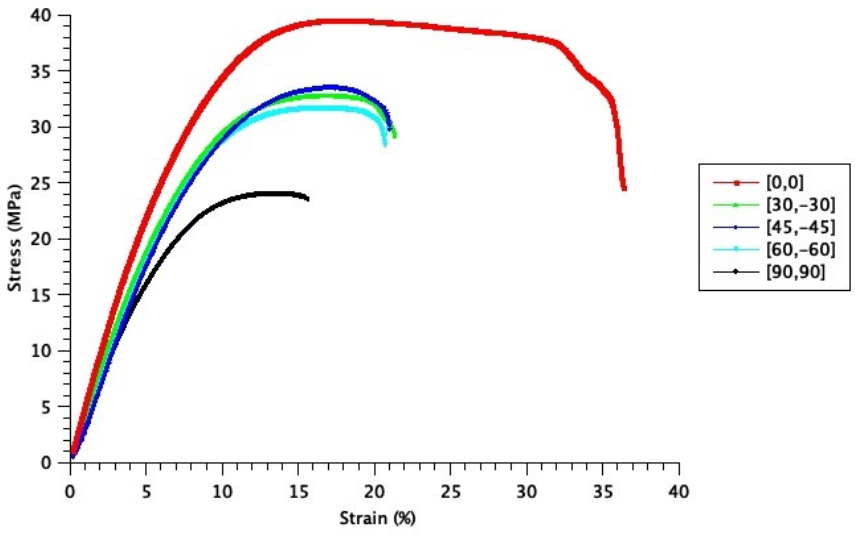

Figure 4.7 Stress-strain curves of specimens with different infill directions

E of the sample was determined from the fitted slope of the linear part in the stress-strain curve, as given by the following formula:

$$E = \frac{\sigma}{\varepsilon} \tag{4.1}$$

where σ is the tensile stress and ε is the uniaxial strain. In Figure 4.8 it can be observed a decreasing trend for E under the different infill directions. In Table 4.3, the numerical values of E are presented for samples with different infill directions. The maximum value (400.75 ± 13.00MPa) was reported at [0,0], while the minimum value (291.80 ± 11.17MPa) was observed at [90,90]; the difference between them was 31.5%. However, the difference of E at [30,-30], [45,-45] and [60,-60] was small, with a maximum difference of 6.3%. It can be concluded that the smaller the angle between infill direction and the load direction, the greater the resistance of the sample to deformation, leading to higher E. Besides, even compared with parts infilled at 0°, E of POM filament was larger, indicating that it was stiffer. It is probably owing to the FDM process, introducing defects, such as voids, warping, etc., which could cause performance degradation.

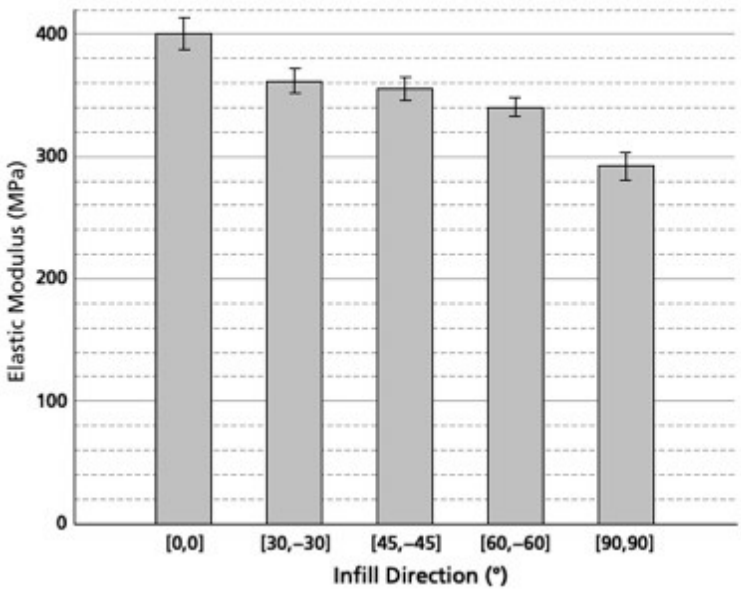

Figure 4.8 Comparison of elastic modulus for different infill directions

Table 4.3 Average elastic modulus (E) and standard deviation of different infill directions

Infill Direction (°)	Elastic Modulus (MPa)	Standard Deviation
[0,0]	400.75	13.00
[30,-30]	361.50	10.21
[45,-45]	355.00	9.25
[60,-60]	340.40	7.77
[90,90]	291.80	11.17

UTS is the maximum stress during the loading process. As shown in Figure 4.9, infill direction had an apparent impact on UTS. It can be noted that under the same condition, UTS increased gradually as the angle of infill direction decreased. The mean values and standard deviations of UTS for the FDM samples prepared from POM are listed in Table 4.4. The highest UTS (40.30 ± 0.76MPa) was found at [0,0], while the lowest value (24.97 ± 0.87MPa) was recorded at [90,90]. For the angle of infill directions less than 45°, UTS dropped 19.9% from 0° to 30°. For the angle of infill directions greater than 45°, UTS dropped 18.2 from 60° to 90°. In addition, the value difference between the part printed in 0° and the filament was small, which shows that their resistance to fracture was similar, thus in some cases, FDM parts can be used instead.

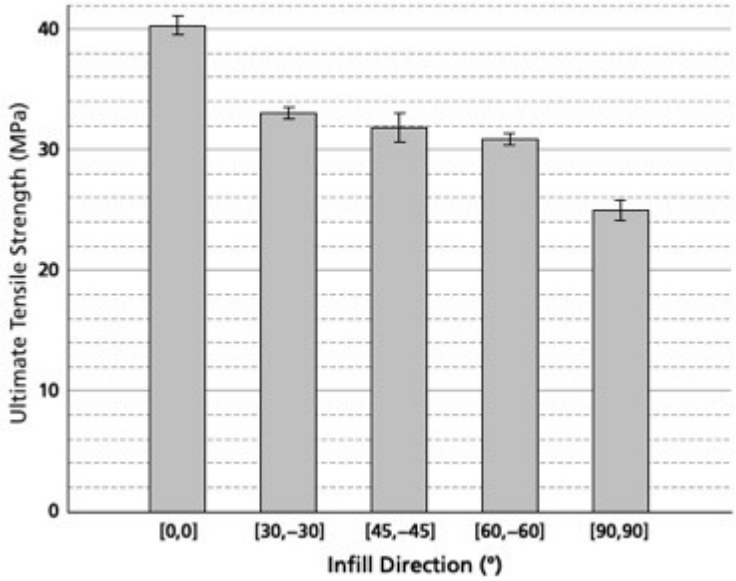

Figure 4.9 Comparison of ultimate tensile strength for different infill directions

Table 4.4 Average ultimate tensile strength (UTS) and standard deviation of different infill directions

Infill Direction (°)	Ultimate Tensile Strength (MPa)	Standard Deviation
[0,0]	40.30	0.76
[30,-30]	33.00	0.47
[45,-45]	31.88	1.20
[60,-60]	30.90	0.46
[90,90]	24.97	0.81

The trend of $EL\%$ with different infill directions is shown in Figure 4.10, which reveals an obvious drop with the increasing angle of the infill direction. Table 4.5 indicates the maximum value was found at 0°, while the minimum value was found at 90°. The mean $EL\%$ shows a reduction of 86.66% between them. It can also be found that when the infill directions of the specimens were close to 45°, their $EL\%$ values were similar. In general, the results revealed that the smaller the angle of infill direction, the better the ductility of the part.

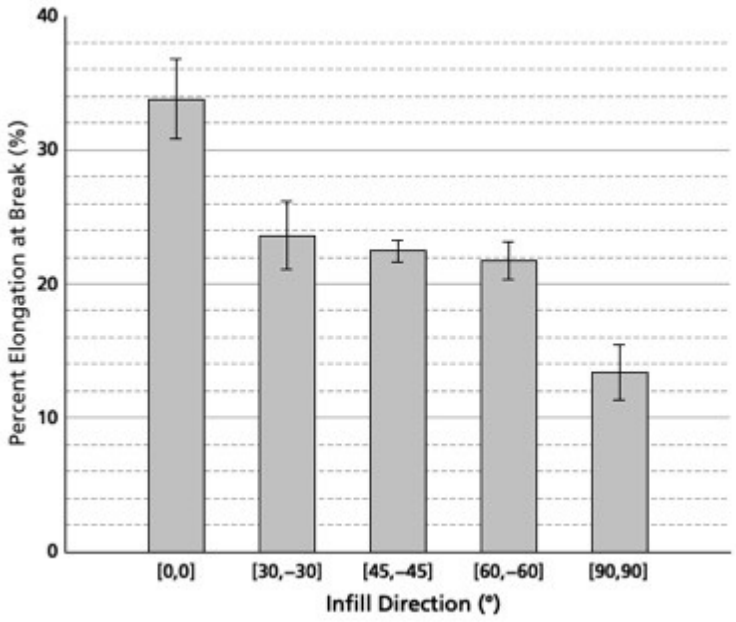

Figure 4.10 Comparison of percent elongation at break for different infill directions

Table 4.5 Average percent elongation at break ($EL\%$) and standard deviation of different infill directions

Infill Direction (°)	Percent Elongation at Break (%)	Standard Deviation
[0,0]	33.79	2.96
[30,-30]	23.63	2.54
[45,-45]	22.46	0.85
[60,-60]	21.73	1.42
[90,90]	13.36	2.06

Wacharawichanant *et al.* studied the mechanical properties of POM samples fabricated via compression molding (CM) and their work reveled that E of POM

sample was about 960MPa, UTS was about 55MPa and $EL\%$ was 37%[82]. Compared with FDM samples, it can be seen that the tensile properties of the CM sample are better. The possible reason for the difference between them is that the CM sample has experienced extreme pressure during the manufacturing process, so that the bonding performance between the materials is better than that of the FDM sample, which results in a better mechanical performance.

In summary, the results reveal that FDM parts exhibit brittleness compared to extruded filament. Due to the unique layer-by-layer production principle of FDM technology, its parts are inherently anisotropic, which means their properties vary with orientation. It confirms that the infill direction had a significant effect on the elastic properties of POM FDM parts, but the effects on the above three parameters were different. Among them, the extent of the impact from the largest to the smallest based on the difference between the maximum and minimum value was $EL\%$, UTS, and E. When the angle of infill direction is the same as the loading angle, the beads bear all the forces, that is, the intermolecular force is the main action. As the angle increases, the component force of the beads and the adhesion between the beads share the load. Once the angle reaches the maximum, only the adhesion force between the beads will bear the load, which is lower than the intermolecular force.

4.3.2 Effect of infill direction on Viscoelastic Properties

Data obtained from DMA tests can be further processed to understand or predict the long-term performance of the material under cycling loading, which is crucial for the application of FDM parts in the industrial field. The storage modulus (G'), the loss modulus (G'') and the loss tangent ($\tan\delta$) were determined from the material response to the sin wave. In the current study, to clearly reveal the relationship between dynamic mechanical performance and temperature, the above three values were described as functions of temperature ($Temp$).

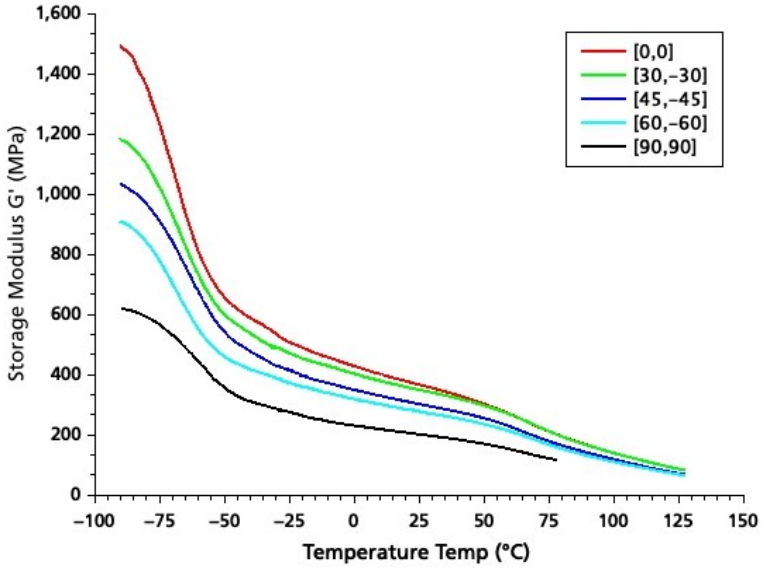

Figure 4.11 Comparison of storage modulus for different infill directions

The variations of G' with temperature for parts with different infill directions are shown in Figure 4.11. G' is an indicator showing the material's ability to store elastic deformation energy, and its value shows a downward trend as the temperature increases. The graph indicates that G' reached its maximum value at the initial temperature, and as the temperature increases, the value of G' of all samples decreases and tends to be consistent. It was observed that the decline rate of G' was large between -90°C and -50°C because the molecular mobility in the polymer chain had been enhanced as the temperature increased[83]. The sample printed at [0,0] shows the highest value of G' throughout the temperature range and followed by [30.-30], [45,45], [60,-60] and [90,90]. The DMA load on the part printed at 0° was perpendicular to the infill direction, so its stiffness was larger than others. Conversely, for the part printed at 90°, the DMA force was parallel to the infill direction, so its stiffness was minimal.

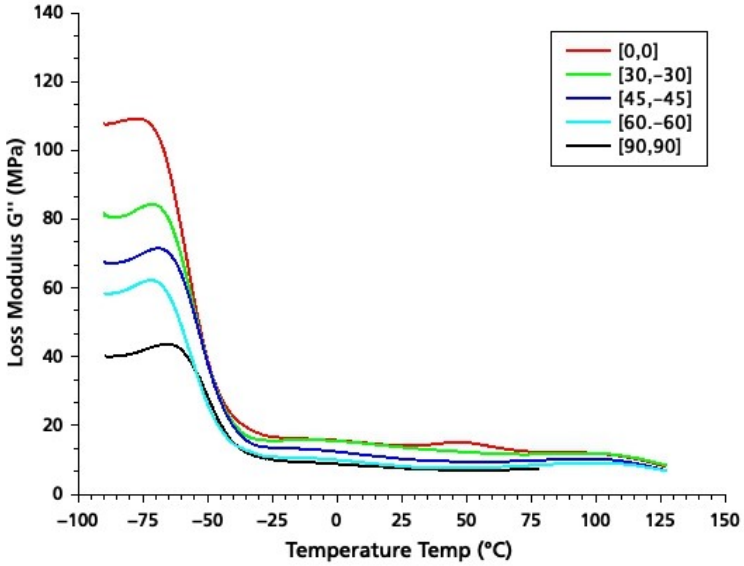

Figure 4.12 Comparison of loss modulus for different infill directions

G'' indicates the viscous properties of a polymer and represents the energy dissipation during the cycling load[84]. Figure 4.12 demonstrates the $G'' - Temp$ curves of parts with different infill directions. In general, regardless of the infill directions, G'' of POM FDM part was lower than its G', which can be regarded as mainly elastic. It must be pointed out that G'' of all samples showed a steady trend at the initial temperature range, i.e., from -85°C to -64°C, and rose to a peak, which indicates the maximum heat dissipation per unit deformation. The trend of the G'' is similar to G': it shows a maximum value at [0,0] and then decreased sequentially with increasing angle of infill direction. Once the beads inside the sample perpendicular to the load direction breaks, it releases more energy than the adhesive layer breaks. However, as the angle of the infill direction increases, the interfacial adhesion between the beads plays a dominant role, while the effect of the intermolecular force decreases. This is probably the explanation for the change in peaks of loss modulus with the variation in infill direction.

Huang *et al.* investigated the dynamic mechanical properties of POM samples obtained via injection molding, and the results showed that the curves of both E' and E'' were similar to those of FDM sample, but the maximum values were

higher[63]. They found that the highest value of G' was about 2100MPa and the highest value of G'' was about 130MPa. As far as the manufacturing method is concerned, IM sample exhibits almost isotropic characteristics while FDM sample exhibits a high degree of anisotropy, which could be an explanation for the difference between. Additionally, parameters of DMA tests such as mode of deformation, heating rate, etc. may affect the final results[85].

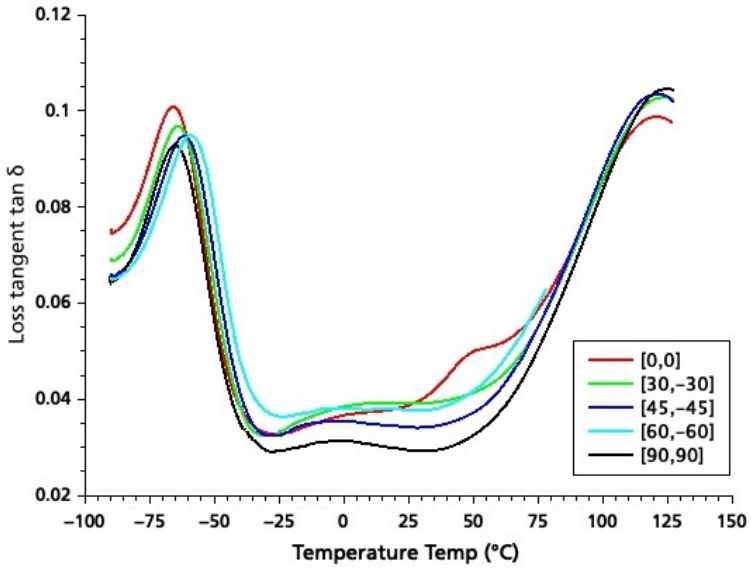

Figure 4.13 Comparison of loss tangent for different infill directions

DMA is one of the techniques to determine the glass transition temperature (T_g) of a material[86]. T_g can be evaluated from the peak of G''or the peak of $\tan\delta$, but in the current work, this value was determined from $\tan\delta - Temp$ curve. $\mathrm{Tan}\ \delta$ is defined as the ratio of G'' to G', which is suitable for determining the occurrence of molecular mobility transition, such as T_g. It can be seen from Figure 4.13 that the change in infill direction had little effect on the peak of $\tan\delta$. In that case, T_g of POM was in the range between -64°C and -61°C. Moreover, the peak ranges of $\tan\delta$ and G'' were very close, so the evaluated T_g can be considered reliable.

To summarize, the dynamic mechanical properties of POM FDM parts strongly depend on the infill direction, which further confirms the anisotropic characteristics of FDM parts.

4.3.3 Shear Properties

Many engineering components, such as shafts, gears, and bearings, etc., are subjected to torsional load during operation. But most of them are made of metals, which are heavy and difficult to process. POM has the potential to become a metal replacement because of its high rigidity and high dimensional accuracy but lightweight. Therefore, it is necessary to explore the shear performance of POM parts made via FDM, which is an indispensable step for replacing industrial metal materials with it in the future. The shear modulus G for a hollow cylinder could be calculated with the following equation:

$$G = TL/J\theta \tag{4.2}$$

where T is the applied torque, L is the length of the specimen, θ is the angle of twist in radians, and J is the polar moment of inertia of the section about its center, can be obtained from the following equation:

$$J = \frac{\pi}{32}(D_0^4 - D_i^4) \tag{4.3}$$

where D_0 is the outer diameter and D_i is the inner diameter of the hollow cylinder. Data obtained from the experiments were plotted, generating a typical function curve of applied torque and the angle of twist shown in Figure 4.14. Torsional stiffness was determined from the linear part of the graph and G was then calculated. The results of the measured diameters and G are shown in the Table 4.6. It can be seen that G of POM FDM part was 89.2 ± 5.7MPa. It should be noted that the print speed needs to be taken into consideration in the manufacturing process of the cylinder, because the faster print speed could affect the adhesion

between layers, thereby reducing the performance. The print speed provided in this work was a balance between efficiency and performance.

Figure 4.14 Representative torque-angle of twist curve of POM FDM parts

Table 4.6 Measurement of diameters and shear modulus of samples

Sample	Outer Diameter D_0 (mm)	Inner Diameter D_i (mm)	Shear Modulus G (MPa)	
			Individual	Intersample
1	8.585	5.965	83.3	
2	8.575	6.121	89.9	
3	8.530	6.020	96.8	89.2 ± 5.7
4	8.595	5.865	92.1	
5	8.505	5.935	84.0	

4.4 Conclusions

This chapter focuses on investigating the influence of infill direction ([0,0], [30,30], [45,-45], [60,-60] and [90,90]) on the elastic and viscoelastic properties of the POM FDM parts. Besides, the shear properties of the POM FDM hollow cylinder were studied as well. The results from the tensile test indicated E of POM FDM parts decreased when the angle of infill direction gradually increased. Similarly, UTS and $EL\%$ showed the same trend with the change of infill direction. The highest

value of E, UTS, and $EL\%$ was obtained at the part printed at [0,0], which were 400.75 ± 13.00MPa, 40.30 ± 0.76MPa, and 33.79 ± 2.96% respectively. While the part infilled with [90,90] showed the lowest E, UTS, and $EL\%$, which were 291.80 ± 11.17MPa, 24.97 ± 0.81MPa, and 13.36 ± 2.06% respectively. The results of DMA confirmed that G' and G'' improved with increasing angle of infill direction. [0,0] sample had the highest G' and G'' and then followed by [30,-30], [45,-45], [60,-60] and [90,90]. It can be concluded that the infill direction had a great influence on both elasticity and viscoelasticity of FDM parts. The results from torsion tests indicate that G of the sample was 89.2 ± 5.7MPa.

This chapter explores the feasibility of POM as an FDM material and provides an analysis of the elastic and viscoelastic properties of POM FDM parts. However, compared with traditional FDM materials, POM still has some drawbacks, such as low friction and high shrinkage rate during the manufacturing process, which can be solved by printing a laminate structure.

Chapter 5 Analysis of the factors affecting the dimensional accuracy of POM FDM parts

5.1 Introduction

The dimensional accuracy of the part is greatly influenced by some specific printing parameters. Dimensional accuracy refers to the match between the actual size of the product and the design size. It is extremely important when FDM parts need to be integrated into larger assemblies precisely[87]. Compared with other plastic molding technologies, the dimensional accuracy of FDM products is relatively low[88]. Therefore, it is worth studying the factors that affect the dimensional accuracy of FDM parts. Kacmarcik *et al.* compared the printing accuracy of the two 3D printers by studying several different geometric characteristics of the PLA FDM reference parts[89]. Soury *et al.* studied the effects of different parameters on the dimensional accuracy of ABS FDM parts through Taguchi's design of experiments and found that the layer thickness and width had an important impact[90]. Basavaraj *et al.* applied the S/N ratio method and reported the best dimensional accuracy of Nylon parts parameter combination was 0.1mm layer thickness, 30° orientation angle and 0.8mm shell thickness[91]. Yang *et al.* revealed the impact of the printing temperature and the speed on the dimensional accuracy of shape memory polymer (SMP) FDM parts[92]. It can be seen that not only the 3D printer but also the materials used will affect the dimensional accuracy of the finished product.

Polyoxymethylene (POM) is a thermoplastic material commonly used to produce functional parts such as gear wheels and ball bearings. It has aroused extensive attention in recent years due to its high stiffness, excellent wear resistance, and good chemical resistance. There are many methods for processing POM, such as injection molding, melt extrusion, solid-state extrusion, blow molding, etc. However, the potential of POM as a 3D printing material in the

FDM field has not yet been fully developed. It is meaningful to investigate the factors affecting the dimensional accuracy of engineering products made of POM.

The objective of the current chapter is to investigate the influence of the size and the printing temperature on the dimensional accuracy of POM FDM parts. Additionally, industrial parts are usually of different shapes, this chapter will also compare the dimensional accuracy of four common shapes: triangle, square, hexagon and circle under the same circumstances.

5.2 Methodology

5.2.1 Materials

POM filament with a diameter around 2.75mm was fabricated via hot melt extrusion (HME) from Chapter 2. Its thermal properties are shown in Table 5.1. PLA filament with a diameter of 2.85mm was purchased from eSUN, and its printing temperature is between 220°C and 260°C.

Table 5.1 Thermal properties of POM filament

Material	**Properties**		
	Shrinkage Value	T_g (°C)	T_m (°C)
POM	2.0	-63	165

5.2.2 Design of Experiments

Design of experiments (DoE) is a systematic method to determine the relationship between input parameters and output corresponding responses[93]. For the purpose of analyzing the effect of the size and the printing temperature on the dimensional accuracy of the specimens, a 2^2 factorial design experiment design was created. Two variables at two levels of this experiment are illustrated in Table 5.2. In order to verify the results and better estimate the influence of experimental factors, each group of experiments was repeated five times, for a total of 20 samples.

Table 5.2 Factors and their levels

Fixed Factors			Control Factors				
						Level	
Factor	**Unit**	**Value**	**Factor**	**Symbol**	**Unit**	**-1**	**1**
Nozzle Diameter	mm	0.4	Size	A	mm	10	20
Build Plate Temperature	°C	60	Printing Temperature	B	°C	210	230
Layer Height	mm	0.3					
Line Width	mm	0.35					
Print Speed	mm/s	40					

5.2.3 Specimen Fabrication via FDM Method

The dimensional accuracy of FDM parts with various shapes is differently affected by external factors. Islam *et al.* examined the linear dimensional error of the square part and the diameter error of the hole part, and discussed their influence on dimensional accuracy[94]. Aslani *et al.* applied the grey-Taguchi method to determine the optimal process parameters for fabricating the rectangular samples with the best dimensional accuracy[95]. However, the dimensional accuracy of parts with other common shapes has not been studied.

In the current work, four different shapes, namely triangle, square, hexagon and circle were printed in two sizes respectively shown in Figure 5.1. In order to reduce the effect of warpage, all POM based samples were printed on a plate made of PLA presented in Figure 5.2. Therefore, a commercial 3D printer named Ultimaker 3 with dual nozzles was used: one of its nozzles was applied to print the PLA plate, while the other was applied to print POM samples.

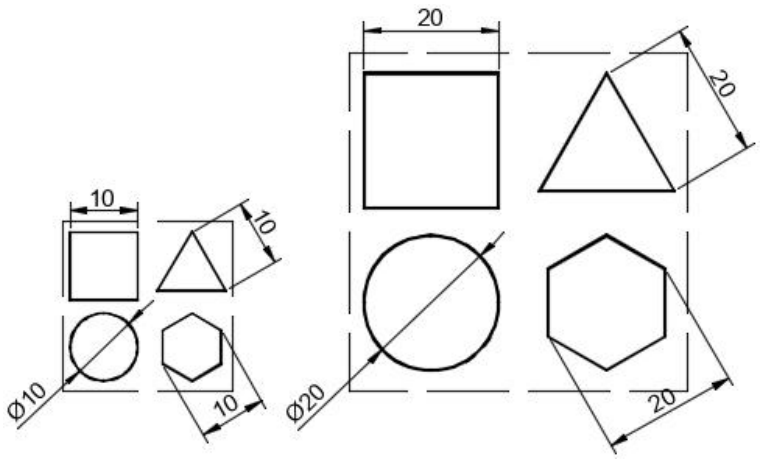

(a) Small size (b) Large size

Figure 5.1 Four different shape in two sizes with dimensions in mm

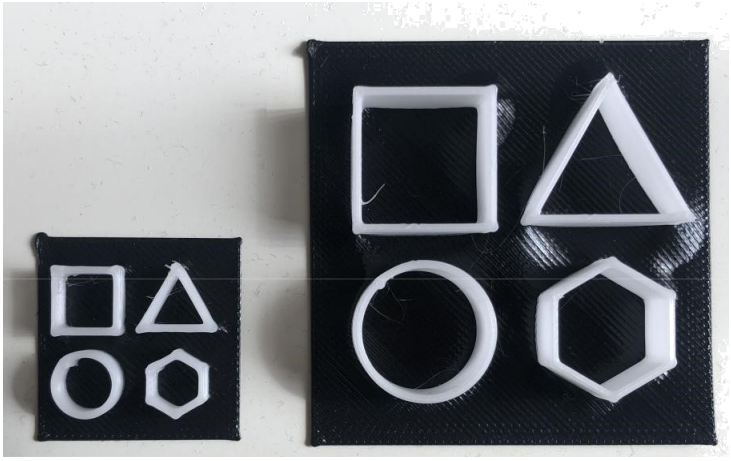

Figure 5.2 Actual FDM samples in two sizes on PLA plates

5.2.4 Measurement

A digital Caliper with a rated accuracy of 0.03mm and a resolution of 0.01mm from Mastercraft was used as the measuring equipment. Measuring the characteristic dimensions of the shape to calculate the perimeter, i.e., the length of three sides of a triangle, the length of four sides of a square, the length of six sides, and the diameter of a circle. Compare the calculated perimeter of each shape with the theoretical value and find the relative error value, which can be calculated from the following equation:

$$RelativeError = \frac{|C_A - C_t|}{C_t} \quad (5.1)$$

Where C_A is the actual perimeter of the shape and C_t is the theoretical perimeter. Relative error is an indicator quantitatively describing the difference between them. In this experiment, the smaller the relative error of the sample, the higher its dimensional accuracy.

5.3 Results and Discussion

Generation of DoE tables and analysis of results were performed in Minitab®. Table 5.3, Table 5.4, Table 5.5 and Table 5.6 show the full factorial design matrix along with the relative error used in this study. First column of table is the non-randomized order of the runs while the second column is the random experiment order. The last column is the response to the input condition.

Table 5.3 Design of Experiment for Triangle

StdOrder	RunOrder	Size	Printing Temperature	Relative Error
19	1	-1	1	0.0475
6	2	1	-1	0.0286
9	3	-1	-1	0.0411
4	4	1	1	0.0228
5	5	-1	-1	0.0378
12	6	1	1	0.0207
15	7	-1	1	0.0483
20	8	1	1	0.0193
16	9	1	1	0.0208
18	10	1	-1	0.0279
8	11	1	1	0.0219
10	12	1	-1	0.0251
1	13	-1	-1	0.0436
11	14	-1	1	0.0544
3	15	-1	1	0.0456
13	16	-1	-1	0.0397
2	17	1	-1	0.0274
14	18	1	-1	0.0224
7	19	-1	1	0.0508
17	20	-1	-1	0.0469

Table 5.4 Design of Experiment for Square

StdOrder	RunOrder	Size	Printing Temperature	Relative Error
17	1	-1	-1	0.0245
6	2	1	-1	0.0183
14	3	1	-1	0.0180
11	4	-1	1	0.0230
10	5	1	-1	0.0198
7	6	-1	1	0.0275
9	7	-1	-1	0.0280
16	8	1	1	0.0148
12	9	1	1	0.0178
5	10	-1	-1	0.0255
15	11	-1	1	0.0350
3	12	-1	1	0.0285
19	13	-1	1	0.0300
13	14	-1	-1	0.0220
1	15	-1	-1	0.0280
4	16	1	1	0.0153
2	17	1	-1	0.0230
8	18	1	1	0.0165
18	19	1	-1	0.0203
20	20	1	1	0.0145

Table 5.5 Design of Experiment for Hexagon

StdOrder	RunOrder	Size	Printing Temperature	Relative Error
10	1	-1	1	0.0042
2	2	-1	1	0.0069
19	3	1	-1	0.0008
6	4	-1	1	0.0089
8	5	1	1	0.0013
16	6	1	1	0.0025
4	7	1	1	0.0015
1	8	-1	-1	0.0081
20	9	1	1	0.0050
13	10	-1	-1	0.0081
11	11	1	-1	0.0023
5	12	-1	-1	0.0112
15	13	1	-1	0.0038
9	14	-1	-1	0.0069
3	15	1	-1	0.0053
7	16	1	-1	0.0015
18	17	-1	1	0.0073
12	18	1	1	0.0005
14	19	-1	1	0.0085
17	20	-1	-1	0.0135

Table 5.6 Design of Experiment for Circle

StdOrder	RunOrder	Size	Printing Temperature	Relative Error
15	1	1	-1	0.0079
3	2	1	-1	0.0002
11	3	1	-1	0.0017
20	4	1	1	0.0004
9	5	-1	-1	0.0094
13	6	-1	-1	0.0049
12	7	1	1	0.0006
8	8	1	1	0.0002
18	9	-1	1	0.0023
4	10	1	1	0.0010
10	11	-1	1	0.0001
5	12	-1	-1	0.0049
14	13	-1	1	0.0001
1	14	-1	-1	0.0090
7	15	1	-1	0.0010
2	16	-1	1	0.0001
16	17	1	1	0.0013
19	18	1	-1	0.0012
17	19	-1	-1	0.0059
6	20	-1	1	0.0043

5.3.1 ANOVA Analysis

In the ANOVA table, the importance of the factor can be determined based on the P-value. Specifically, when the P-value is less than α (0.05 in this experiment), the differences between the means are statistically significant. From the analysis results for triangle presented in Table 5.7, it indicates that the size and the two-way interaction were statistically significant. At the same time, it also shows that the size exerted the most significant effect on the dimensional accuracy because the F-Value of it was higher than the other factors. From the analysis results for square in Table 5.8, the dimensional accuracy was significantly determined by the size and the interaction. From the analysis results for hexagon in Table 5.9, it can be found that only the size affected the dimensional accuracy. From the analysis results for circle in Table 5.10, it implies that both the size and the printing temperature affected the dimensional accuracy significantly, but the printing temperature had a greater influence.

Table 5.7 ANOVA table for Triangle

Source	DF	Adj SS	Adj MS	F-Value	P-Value
Model	3	0.000509	0.00017	21.83	0.000
Linear	2	0.000443	0.000221	28.47	0.000
Size	1	0.000442	0.000442	56.8	0.000
Printing Temperature	1	0.000001	0.000001	0.13	0.723
2-Way Interactions	1	0.000067	0.000067	8.56	0.010
Size*Printing Temperature	1	0.000067	0.000067	8.56	0.010
Error	16	0.000124	0.000008		
Total	19	0.000634			

Table 5.8 ANOVA table for Square

Source	DF	Adj SS	Adj MS	F-Value	P-Value
Model	3	0.002603	0.000868	106.27	0.000
Linear	2	0.002402	0.001201	147.12	0.000
Size	1	0.002396	0.002396	293.4	0.000
Printing Temperature	1	0.000007	0.000007	0.83	0.375
2-Way Interactions	1	0.000201	0.000201	24.56	0.000
Size*Printing Temperature	1	0.000201	0.000201	24.56	0.000
Error	16	0.000131	0.000008		
Total	19	0.002734			

Table 5.9 ANOVA table for Hexagon

Source	DF	Adj SS	Adj MS	F-Value	P-Value
Model	3	0.000191	0.000064	15.04	0.000
Linear	2	0.000186	0.000093	22.06	0.000
Size	1	0.000176	0.000176	41.57	0.000
Printing Temperature	1	0.000011	0.000011	2.55	0.130
2-Way Interactions	1	0.000004	0.000004	1.00	0.333
Size*Printing Temperature	1	0.000004	0.000004	1.00	0.333
Error	16	0.000068	0.000004		
Total	19	0.000258			

Table 5.10 ANOVA table for Circle

Source	DF	Adj SS	Adj MS	F-Value	P-Value
Model	3	0.000113	0.000038	8.23	0.002
Linear	2	0.000096	0.000048	10.44	0.001
Size	1	0.000033	0.000033	7.08	0.017
Printing Temperature	1	0.000063	0.000063	13.8	0.002
2-Way Interactions	1	0.000017	0.000017	3.8	0.069
Size*Printing Temperature	1	0.000017	0.000017	3.8	0.069
Error	16	0.000074	0.000005		
Total	19	0.000187			

5.3.2 Main Effects

In a multi-level experiment with several factors, the main effects plot is used to describe how much a factor affects the amount of response at each level. From Figure 5.3(a), it can be found that the slope of the size is steeper, indicating that it had a greater impact on dimensional accuracy of triangle. From Figure 5.3(b), it shows the slope of the size is steeper, implying that it affected the dimensional accuracy of square more than the printing temperature. Figure 5.3(c) shows that the size was the dominant factor affecting the dimensional accuracy of hexagon. Figure 5.3(d) illustrate that the effect of the printing temperature was greater than the size for circle. In general, for triangle, square, and hexagon, the size would directly affect the dimension accuracy while for circle, it was the printing temperature.

It must be pointed out that when the printing temperature was lower than 210°C, both triangle and square had apparent delamination, as shown in Figure 5.4. This was another reason for low dimensional accuracy, but it cannot be described by measurement, so the printing temperature in this work was higher than 210°C.

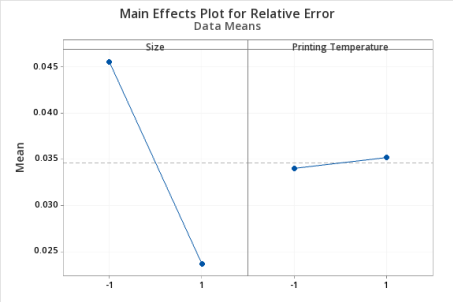

(a) Main Effects Plot for Triangle

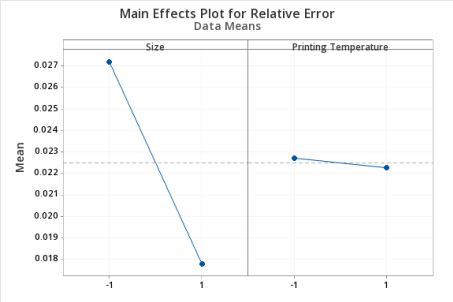

(b) Main Effects Plot for Square

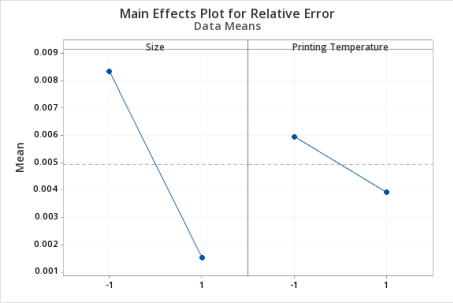

(c) Main Effects Plot for Hexagon

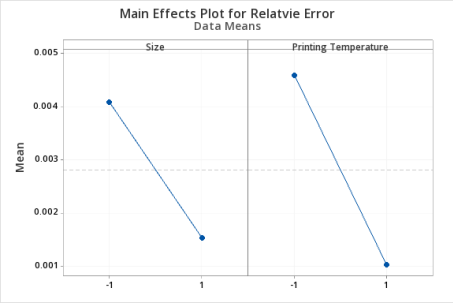

(d) Main Effects Plot for Circle

Figure 5.3 Main Effects Plot for Relative Error

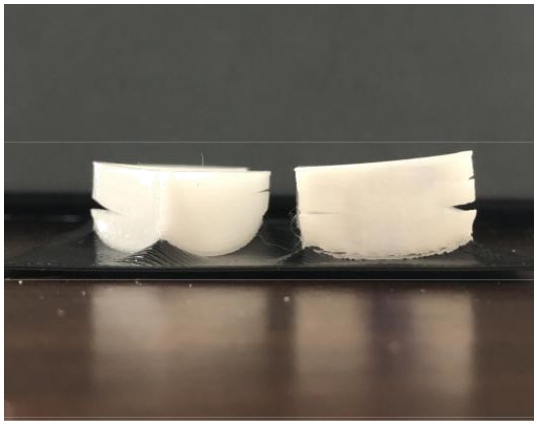

Figure 5.4 Delamination between layers for Triangle and Square

5.3.3 Interaction

The interaction plot is applied to show how the relationship between a category factor and continuous response depends on the value of the second category factor. Figure 5.5(a) and Figure 5.5(b) reveal a similar interaction trend: the interaction shows moderate reversal. It can be noticed a difference between the size when the printing temperature is at a low level, but that difference is reinforced when the printing temperature is at a high level for each size.

The parallel lines in Figure 5.5(c) imply that there is no interaction effect for hexagon and the main effect is the size, which was confirmed in Table 5.9.

The near-parallel lines in Figure 5.5(d) suggest that there is no interaction effect for circle, which was confirmed in Table 5.10. The graph shows that the relative error levels are lower for both in the small and large size when the printing temperature was high.

For both triangle and square, the large size and the high printing temperature can result in the smallest relative error, while the small size and the high printing temperature can cause the largest relative error. For hexagon, the smallest relative error was at the large size and the high printing temperature, while the largest relative error was at the small size and the low printing temperature. For

circle, at the high printing temperature, the large size caused the smallest relative error, while at the low printing temperature, the small size led to the largest relative error.

It can be concluded that for all four shapes, the larger the size, the higher the dimensional accuracy. But for different shapes, the effect of the printing temperature was different.

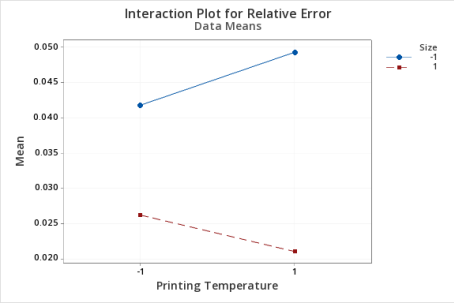

(a) Interaction Plot for Triangle

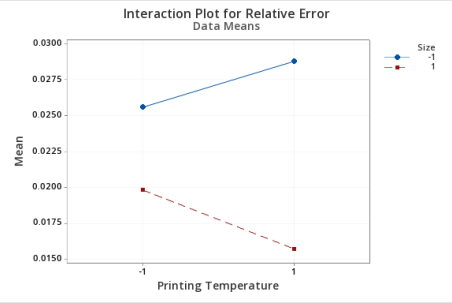

(b) Interaction Plot for Square

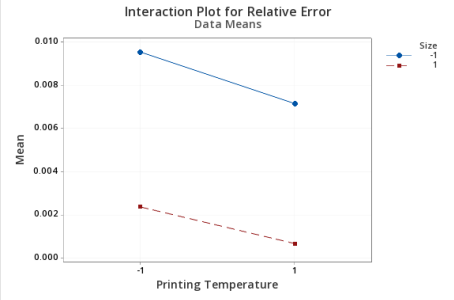

(c) Interaction Plot for Hexagon

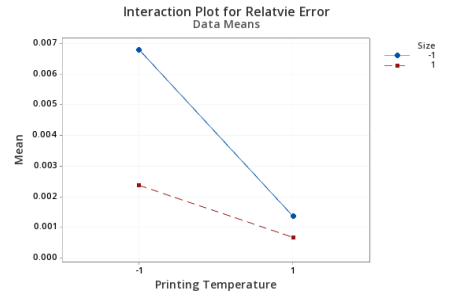

(d) Interaction Plot for Circle

Figure 5.5 Interaction Plot for Relative Plot

5.3.4 Regression Models for Relative Error

On the basis experimental data obtained, statistic regressions have been done to explain the correlation of different parameters and their corresponding responses. As mentioned in Table 5.2, the letter A represents the size while the letter B represents the printing temperature.

The factorial regression model for triangle given in terms of uncoded units is as follows:

$$RelativeError = 0.034639 - 0.010944 \times A + 0.000583 \times B - 0.003167 \times A \times B \quad (5.2)$$

The factorial regression model for square given in terms of uncoded units is as follows:

$$RelativeError = 0.022500 - 0.004700 \times A + 0.000225 \times B - 0.001825 \times A \times B \quad (5.3)$$

The factorial regression model for hexagon given in terms of uncoded units is as follows:

$$RelativeError = 0.004946 - 0.003406 \times A + 0.001020 \times B + 0.000173 \times A \times B \quad (5.4)$$

The factorial regression model for circle given in terms of uncoded units is as follows:

$$RelativeError = 0.003257 - 0.000833 \times A + 0.001495 \times B + 0.001220 \times A \times B \quad (5.5)$$

Table 5.11 Regression analysis summary

Shape	Standard Deviation	R^2 (adj)	R^2 (pred)
Triangle	0.0028715	52.52%	37.53%
Square	0.0022682	70.89%	61.70%
Hexagon	0.0027889	76.69%	69.32%
Circle	0.0028575	94.32%	92.53%

Table 5.11 summarizes the coefficients of determination for all shapes. R^2 is a statistical value used to describe the degree of fitting of the equation. In general, the higher the R^2, the better the model fits the data.

The above fitted models can be applied to roughly predict the dimensional accuracy of four different shapes within an acceptable range. The feasibility of fitting equations of different shapes from high to low is circle, hexagon, square and triangle.

5.3.5 Difference in dimensional accuracy between different shapes

Figure 5.6 show the analysis results of fabricated shapes under the same conditions. It can be clearly seen from Figure 5.6(a) and Figure 5.6(b) that in the case of small size, no matter how the printing temperature changed, the relative error of circle was the smallest while the relative error of triangle was the largest. Figure 5.6(c) and Figure 5.6(d) reveal the same trend when printed in large size. When the printing temperature was the same, regardless of the size, the relative error from small to large was circle, hexagon, square and triangle. In addition, all figures indicate that the difference between the relative error of hexagon and circle was small.

For shapes with fewer sides, such as triangle and square, the relative error of them were larger. This may be due to their poor adhesion between the sides and the bottom. Therefore, it can be considered that when the shape of the part is closer to the circle, the relative error is smaller, and the dimensional accuracy is higher.

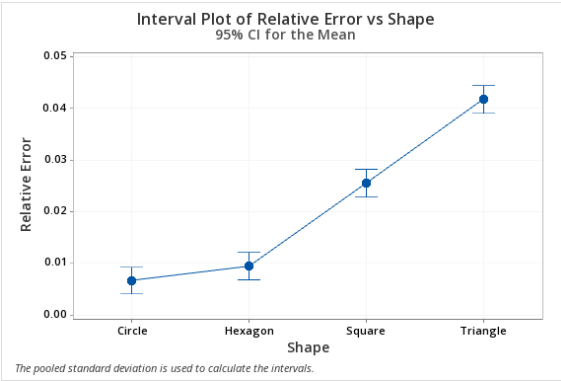

(a) Small size and Low printing temperature

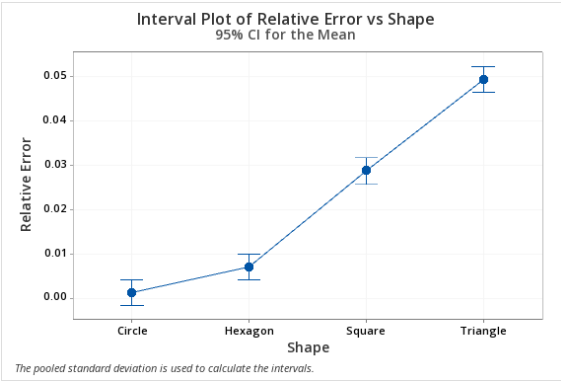

(b) Small size and High printing temperature

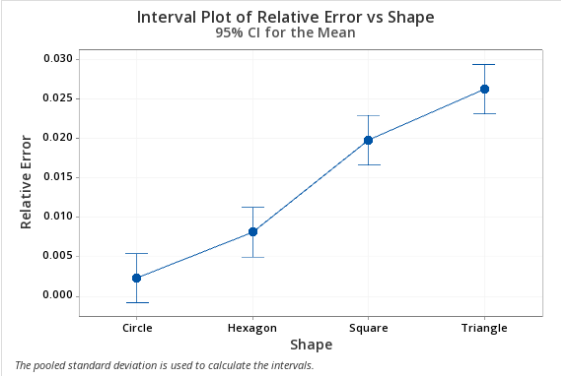

(c) Large size and Low printing temperature

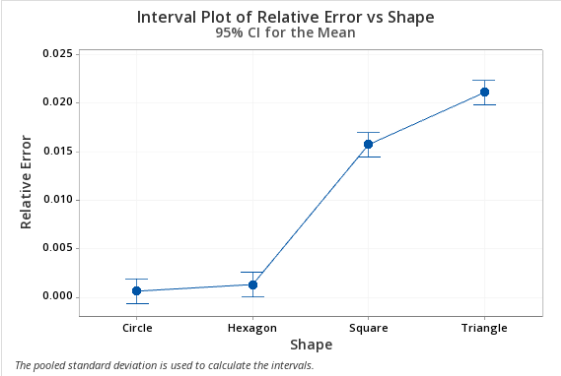

(d) Large size and High printing temperature

Figure 5.6 Interval Plot for Relative Error

5.4 Conclusions

The effect of the size and the printing temperature on the dimensional accuracy of POM FDM parts with different shapes was investigated. A 2^2 design of experiment was conducted with five replicates for each shape. The parameters adjusted during the printing process were the size, printing temperature and the shape of the sample. Both the size and the printing temperature had two levels, while the shape was assigned four levels to be tested. Test results were then analyzed using ANOVA to determine the influence of each factor and their interactions. In addition to the circle, the most important factor affecting the dimensional accuracy of other shapes was the size. It can be found that for triangle and square, the interaction of the parameters had the same trend: there may be a moderate reversal, while for circle, the overall trend of the interaction was the same. To better understand the influence of parameters, four simple regression models had been generated to predict the dimensional accuracy of different shapes. The two variables in the models are the size and the printing temperature. According to the analysis of different shapes, it indicates that the more the sides of the shape, the higher the dimensional accuracy it achieves. As a consequence, FDM technology is more suitable for the production of near-round POM components such as gears and shafts.

Further research will focus on investigating other factors, such as print speed and build plate temperature that may affect the dimensional accuracy of POM FMD parts.

Chapter 6 Summary and Future Works

6.1 Summary of the Thesis

In this study, POM filament was successfully fabricated for FDM via the melt extrusion. The process parameters were studied carefully, and the optimal parameters combination was selected. Later, 3D printing of POM parts was done, and mechanical and thermomechanical properties of the said parts were documented. The key points are summarized as follows:

- TGA and DSC (POM filaments)
  The results showed that POM started to decompose at 252°C and completely decomposed at 408°C. It was observed that the T_m of the POM was 165°C, and the X_c was 49.7%.

- Mechanical properties (POM filaments)
  It was found that the elastic modulus was 1.27 ± 0.13MPa, the elongation at yield was 2.32 ± 0.07% and the ultimate tensile strength was 42.15 ± 2.77MPa.

As an engineering material, POM is rarely used in FDM manufacturing, but as the demand for rapid production increases day by day, it is necessary to study the performance of POM FDM parts. This thesis highlights the detailed insights into properties of POM FDM parts.

- Elastic Properties
  By analyzing the stress-strain curves, three typical elastic properties, i.e., E, UTS, and $EL\%$, have been investigated on the samples with different infill directions. For uniaxial tensile testing, as expected, the sample with 0° presented the best mechanical performance in terms of E, UTS and $EL\%$.

Elastic performance decreased with the increasing angle of infill direction due to the reduced load-bearing capacity of the beads.

- Viscoelastic Properties

  In DMA tests, G', G'' and $\tan\delta$ were plotted as functions of temperature. The results indicate that [0,0] samples provided the highest value of G' and G''. This was followed by [30, -30], [45,-45], [60,-60] and [90,90] samples. It was confirmed that the infill direction remarkably affected the viscoelastic properties of POM FDM parts. T_g of POM determined from $\tan\delta - Temp$ curves was between -64°C and -61°C.

- Shear Properties

  Through conducting torsion tests on the hollow cylinder, it was determined that the shear modulus of FDM produced POM was 89.2 ± 5.7MPa.

It is necessary to conduct an in-depth study on the dimensional accuracy of POM FDM parts to popularize the use of them in the industrial fields. A preliminary work to highlight the differences in dimensional accuracy of different shapes was also studied.

- Effect of the Size and the Printing Temperature

  Four different shapes of samples were printed to investigate the effect of the size and the printing temperature on dimensional accuracy. It was found that the size had a dominant influence on the dimensional accuracy of triangle, square, and hexagon, while for circle, it was the printing temperature.

- Effect of the Shape

  Under various printing conditions, the dimensional accuracy of different shapes showed a similar trend, from high to low was circle, hexagon, square and triangle. Therefore, it can be considered that the shape of the part is close to a circle, the higher the dimensional accuracy it could achieve. This discovery can provide advice and guidance for the design of industrial parts.

As a final note, the study was affected by the COVID-19 crisis around the world. Some of the intended work had to be left out due to time and laboratory accessibility.

6.2 Potential Future Work Recommendations

1. Fabrication of POM filaments mixed with other materials

   The applications of POM have limitations due to POM's inherent brittle behavior and thermal instability[96]. Many studies have shown that POM-based nanocomposites can achieve superior performance and broader applications compared to that of traditional POM materials. Kumar et al. studied the influence of adding thermoplastic polyurethane (TPU) in POM/TPU blends and reported that adding TPU can significantly improve the fracture performance of the blends[97]. Mixing POM with other nanocomposites is an effective and economical method to improve its properties, which will be a valuable research direction.

2. The laminated structure of POM and other materials

   POM does not adhere well to any of the typical build plate surface. However, it can be observed that POM has good adhesion to materials such as PLA or ABS. In that case, printing a laminated structure is an effective way to solve the problem. Therefore, it is worthwhile to investigate the performance of components composed of laminated structures of POM and other materials.

3. Influence of other factors on the dimensional accuracy

   More process factors, such as print speed, infill density, and infill pattern should be investigated to explore their impact on the dimensional accuracy of POM FDM parts.

Bibliography

[1] J. Lee, A. R. Unnithan, C. H. Park, and C. S. Kim, “3D bioprinting for active drug delivery,” in *Biomimetic Nanoengineered Materials for Advanced Drug Delivery*, Elsevier Inc., 2019, pp. 61–72.

[2] Z.-X. Low, Y. T. Chua, B. M. Ray, D. Mattia, I. S. Metcalfe, and D. A. Patterson, “Perspective on 3D printing of separation membranes and comparison to related unconventional fabrication techniques,” *J. Memb. Sci.*, vol. 523, no. May 2016, pp. 596–613, Feb. 2017.

[3] B. M. Tymrak, M. Kreiger, and J. M. Pearce, “Mechanical properties of components fabricated with open-source 3-D printers under realistic environmental conditions,” *Mater. Des.*, vol. 58, pp. 242–246, Jun. 2014.

[4] J. Raasch, M. Ivey, D. Aldrich, D. S. Nobes, and C. Ayranci, “Characterization of polyurethane shape memory polymer processed by material extrusion additive manufacturing,” *Addit. Manuf.*, vol. 8, pp. 132–141, Oct. 2015.

[5] S. Lüftl, V. P.M., and S. Chandran, Eds., *Polyoxymethylene Handbook*. Hoboken, NJ, USA: John Wiley & Sons, Inc., 2014.

[6] C. V Pious and S. Thomas, “2 - Polymeric Materials—Structure, Properties, and Applications,” in *Printing on Polymers*, J. Izdebska and S. Thomas, Eds. William Andrew Publishing, 2016, pp. 21–39.

[7] D. Henrist and J. . Remon, “Influence of the process parameters on the characteristics of starch based hot stage extrudates,” *Int. J. Pharm.*, vol. 189, no. 1, pp. 7–17, Oct. 1999.

[8] A. Savini and G. G. Savini, “A short history of 3D printing, a technological revolution just started,” in *2015 ICOHTEC/IEEE International History of High-Technologies and their Socio-Cultural Contexts Conference (HISTELCON)*, 2015, pp. 1–8.

[9] D. E. H. Jones, “Ariadne,” *New Sci.*, vol. 3, p. 80, 1974.

[10] T. Birtchnell and W. Hoyle, *3D Printing for Development in the Global South*. London: Palgrave Macmillan UK, 2014.

[11] B. Huang and S. Singamneni, “Adaptive slicing and speed- and time-dependent consolidation mechanisms in fused deposition modeling,” *Proc. Inst. Mech. Eng. Part B J. Eng. Manuf.*, vol. 228, no. 1, pp. 111–126, Jan. 2014.

[12] P. Shubham, C. Aggarwal, and S. Joshi, “Optimization of Process Parameter to Improve Dynamic Mechanical Properties of 3D Printed ABS Polymer using Taguchi Method,” *Int. J. Mech. Prod. Eng.*, no. 6, pp. 2321–2071, 2018.

[13] Abdul W. Basit and Simon Gaisford, *3D printing of Pharmaceuticals*. 2018.

[14] H. C. W, “Apparatus For Production Of Three-dimensional Objects By Stereolithography,” 1986.

[15] Y. Yan *et al.*, “Rapid prototyping and manufacturing technology: Principle, representative technics, applications, and development trends,” *Tsinghua Sci. Technol.*, vol. 14, no. S1, pp. 1–12, Jun. 2009.
[16] F. MICHAEL, “Apparatus And Method For Forming An Integral Object From Laminations,” 1988.
[17] Wohlers Associates Inc., “Wohler’s report 2015 - 3D printing and additive manufacturing state of the industry. Annual Worldwide Progress Report.,” 2015.
[18] T. Chartier and A. Badev, “Rapid Prototyping of Ceramics,” in *Handbook of Advanced Ceramics: Materials, Applications, Processing, and Properties: Second Edition*, Second Edi., Elsevier, 2013, pp. 489–524.
[19] A. 52900:2015, “Standard Terminology for Additive Manufacturing – General Principles – Terminology,” *ASTM Int.*, vol. i, pp. 1–9, 2015.
[20] J. P. Kruth, “Material Incress Manufacturing by Rapid Prototyping Techniques,” *CIRP Ann.*, vol. 40, no. 2, pp. 603–614, 1991.
[21] W. Zhu, J. G. Ock, X. Ma, W. Li, and S. Chen, “3D Printing and Nanomanufacturing,” in *3D Bioprinting and Nanotechnology in Tissue Engineering and Regenerative Medicine*, Elsevier Inc., 2015, pp. 25–55.
[22] P. Kulkarni, A. Marsan, and D. Dutta, “A review of process planning techniques in layered manufacturing,” *Rapid Prototyp. J.*, vol. 6, no. 1, pp. 18–35, Mar. 2000.
[23] I *et al.*, “Advanced Design for Additive Manufacturing: 3D Slicing and 2D Path Planning,” in *Colloids and Surfaces A: Physicochemical and Engineering Aspects*, vol. 395, no. tourism, 2012, pp. 116–124.
[24] W. Oropallo and L. A. Piegl, “Ten challenges in 3D printing,” *Eng. Comput.*, vol. 32, no. 1, pp. 135–148, 2016.
[25] Z. Zhang and S. Joshi, “An improved slicing algorithm with efficient contour construction using STL files,” *Int. J. Adv. Manuf. Technol.*, vol. 80, no. 5–8, pp. 1347–1362, 2015.
[26] K. G. Mostafa, C. Montemagno, and A. J. Qureshi, “Strength to cost ratio analysis of FDM Nylon 12 3D Printed Parts,” *Procedia Manuf.*, vol. 26, pp. 753–762, 2018.
[27] L. Novakova-Marcincinova, J. Novak-Marcincin, J. Barna, and J. Torok, “Special materials used in FDM rapid prototyping technology application,” in *2012 IEEE 16th International Conference on Intelligent Engineering Systems (INES)*, 2012, pp. 73–76.
[28] S. Menderes, KAM, Ahmet, İPEKÇİ, Hamit, “Investigation of 3D Printing Occupancy Rates Effect on Mechanical Properties and Surface Roughness of PET-G Material Products,” *J. New Results Sci.*, vol. 7, no. 2, pp. 1–8, 2018.
[29] R. Singh and S. Singh, “Development of Nylon Based FDM Filament for Rapid Tooling Application,” *J. Inst. Eng. Ser. C*, vol. 95, no. 2, pp. 103–108, Apr. 2014.
[30] H. Klippstein, A. Diaz De Cerio Sanchez, H. Hassanin, Y. Zweiri, and L. Seneviratne, “Fused Deposition Modeling for Unmanned Aerial Vehicles (UAVs): A Review,” *Adv. Eng. Mater.*, vol. 20, no. 2, p. 1700552, Feb. 2018.
[31] C. Esposito Corcione, E. Palumbo, A. Masciullo, F. Montagna, and M. C. Torricelli, “Fused Deposition Modeling (FDM): An innovative technique aimed at reusing Lecce stone waste for industrial design and building applications,” *Constr. Build. Mater.*, vol. 158, pp. 276–284, 2018.

[32] D. Khorsandi, A. Fahimipour, S. S. Saber, A. Ahmad, and A. A. De Stephanis, “Fused Deposition Modeling and Stereolithography 3D Bioprinting in Dental Science,” *EC Dent. Sci.*, vol. 18, no. 2019, pp. 110–115, 2019.
[33] S. H. Masood, “Application of fused deposition modelling in controlled drug delivery devices,” *Assem. Autom.*, vol. 27, no. 3, pp. 215–221, Aug. 2007.
[34] “Recommended Wall Thickness for 3D Printing | Fictiv - Hardware Guide.” [Online]. Available: https://www.fictiv.com/hwg/fabricate/recommended-wall-thickness-for-3d-printing. [Accessed: 13-Aug-2020].
[35] D.-H. You, “Optimal Printing Conditions of PLA Printing Material for 3D Printer,” *Trans. Korean Inst. Electr. Eng.*, vol. 65, no. 5, pp. 825–830, May 2016.
[36] O. Lužanin, D. Movrin, and M. Plan, “Experimental Investigation of Extrusion Speed and Temperature Effects on Arithmetic Mean Surface Roughness in Fdm-,” *J. Technol. Plast.*, vol. 38, no. 2, pp. 179–190, 2013.
[37] “Ultimaker Cura: Powerful, easy-to-use 3D printing software.” [Online]. Available: https://ultimaker.com/software/ultimaker-cura. [Accessed: 07-Aug-2020].
[38] S. Rohde *et al.*, “Experimental Characterization of the Shear Properties of 3D–Printed ABS and Polycarbonate Parts,” *Exp. Mech.*, vol. 58, no. 6, pp. 871–884, Jul. 2018.
[39] N. Ayrilmis, “Effect of layer thickness on surface properties of 3D printed materials produced from wood flour/PLA filament,” *Polym. Test.*, vol. 71, no. July, pp. 163–166, Oct. 2018.
[40] D. Croccolo, M. De Agostinis, and G. Olmi, “Experimental characterization and analytical modelling of the mechanical behaviour of fused deposition processed parts made of ABS-M30,” *Comput. Mater. Sci.*, vol. 79, pp. 506–518, 2013.
[41] S. F. Khan, H. Zakaria, Y. L. Chong, M. A. M. Saad, and K. Basaruddin, “Effect of infill on tensile and flexural strength of 3D printed PLA parts,” *IOP Conf. Ser. Mater. Sci. Eng.*, vol. 429, no. 1, p. 012101, Nov. 2018.
[42] J. F. M. Fernandes, “Study of the influence of 3D printing parameters on the mechanical properties of PLA,” *Proc. Int. Conf. Prog. Addit. Manuf.*, vol. 2018-May, pp. 547–552, 2018.
[43] M. Somireddy, D. A. De Moraes, and A. Czekanski, “Flexural Behavior of Fdm Parts: Experimental, Analytical and Numerical Study,” *Solid Free. Fabr. Symp.*, no. March 2018, pp. 992–1004, 2017.
[44] H. M. Leicester, “Alexander Mikhaĭlovich Butlerov,” *J. Chem. Educ.*, vol. 17, no. 5, p. 203, May 1940.
[45] W. Heuer, “Über synthetische hochmolekulare Stoffe,” in *Die Hochmolekularen Organischen Verbindungen*, vol. 145, no. 1929, Berlin, Heidelberg: Springer Berlin Heidelberg, 1932, pp. 157–377.
[46] B.-W. FREIBURG, “THE FOUNDATION OF POLYMER SCIENCE BY HERMANN STAUDINGER (1881-1965),” 1999.
[47] “Concluding Thoughts,” in *How to Invent and Protect Your Invention*, John Wiley & Sons, Ltd, 2012, pp. 131–138.
[48] K. J. Persak and R. A. Fleming, *High Performance Polymers: Their Origin and Development*. Dordrecht: Springer Netherlands, 1986.
[49] C. C. Ibeh, *Thermoplastic Materials : Properties, Manufacturing Methods, and Applications*. Baton Rouge, UNITED STATES: CRC Press LLC, 2011.

[50] G. S. Heinlein and S. J. Timpe, “Development of elastic and plastic properties of polyoxymethylene during bending fatigue,” *J. Appl. Polym. Sci.*, vol. 131, no. 18, p. n/a-n/a, Sep. 2014.
[51] “Materials Database.” [Online]. Available: http://tools.ticona.com/. [Accessed: 13-Aug-2020].
[52] R. W. Hertzberg, M. D. Skibo, and J. A. Manson, “Fatigue crack propagation in polyacetal,” *J. Mater. Sci.*, vol. 13, no. 5, pp. 1038–1044, May 1978.
[53] W. H. Stockmayer and L.-L. Chan, “Solution properties of polyoxymethylene,” *J. Polym. Sci. Part A-2 Polym. Phys.*, vol. 4, no. 3, pp. 437–446, Jun. 1966.
[54] F. Yang, H. Li, L. Cai, F. Lan, and M. Xiang, “Degradation and Stabilization of Co-POM,” *Polym. Plast. Technol. Eng.*, vol. 48, no. 5, pp. 530–534, May 2009.
[55] R. Recovery, C. Molded, and B. T. Specimens, “Standard Classification System and Basis for Specification for Polyoxymethylene Molding and Extrusion Materials (POM) 1,” pp. 1–7, 2012.
[56] “Global Polyoxymethylene (POM) Market 2020| Industry Demand, Share, Global Trend, Industry News, Business Growth, Top Key Players Update, Business Statistics and Research Methodology by Forecast to 2023 - Market Research Posts.” [Online]. Available: https://marketresearchposts.com/2020/07/25/global-polyoxymethylene-pom-market-2020-industry-demand-share-global-trend-industry-news-business-growth-top-key-players-update-business-statistics-and-research-methodology-by-forecast-to-202/. [Accessed: 26-Jul-2020].
[57] Cavenett, *Handbook of Thermoplastics*, vol. 53, no. 9. Cambridge: CRC Press, 2016.
[58] G. Properties, “General Properties of System Matrix 1 General Properties of System.”
[59] K. R. Rajisha, B. Deepa, L. A. Pothan, and S. Thomas, “9 - Thermomechanical and spectroscopic characterization of natural fibre composites,” in *Interface Engineering of Natural Fibre Composites for Maximum Performance*, N. E. Zafeiropoulos, Ed. Woodhead Publishing, 2011, pp. 241–274.
[60] R. Sindhu, P. Binod, and A. Pandey, “Chapter 17 - Microbial Poly-3-Hydroxybutyrate and Related Copolymers,” in *Industrial Biorefineries & White Biotechnology*, A. Pandey, R. Höfer, M. Taherzadeh, K. M. Nampoothiri, and C. Larroche, Eds. Amsterdam: Elsevier, 2015, pp. 575–605.
[61] Y. Aoki, A. Nobuta, A. Chiba, and M. Kaneko, “Study of Glass Transition and Partial Melting in Melt-crystallized Poly(oxymethylene) by X-Ray Small-angle Scattering,” *Polym. J.*, vol. 2, no. 4, pp. 502–508, Jul. 1971.
[62] Y. Kong and J. N. Hay, “The measurement of the crystallinity of polymers by DSC,” *Polymer (Guildf).*, vol. 43, no. 14, pp. 3873–3878, Jun. 2002.
[63] T. Huang, R. Lu, H. Wang, Y. Ma, J. Tian, and T. Li, “Investigation on the Tribological Properties of POM Modified by Nano-PTFE,” *J. Macromol. Sci. Part B*, vol. 50, no. 7, pp. 1235–1248, Jul. 2011.
[64] S. Wacharawichanant, P. Amorncharoen, and R. Wannasirichoke, “Effects of Compatibilizer on the Properties of Polyoxymethylene/Acrylonitrile-Butadiene-Styrene Blends,” *Adv. Mater. Res.*, vol. 1052, pp. 220–225, Oct. 2014.
[65] “Polyoxymethylene - Homopolymer - online catalogue source - supplier of research materials in small quantities - Goodfellow.” [Online]. Available:

http://www.goodfellow.com/E/Polyoxymethylene-Homopolymer.html. [Accessed: 27-Aug-2020].
[66] S. M. M. Sabet *et al.*, “Friction Properties of Polyoxymethylene (POM) Materials in Dry and Lubricated Conditions,” in *Lecture Notes in Electrical Engineering*, vol. 505, 2019, pp. 568–573.
[67] Y. Pagnis, *Engineering thermoplastics*, vol. 25, no. Annual. 1990.
[68] I. Muro-Fraguas, E. Sainz-García, A. Pernía-Espinoza, and F. Alba-Elías, “Atmospheric pressure air plasma treatment to improve the 3D printing of polyoxymethylene,” *Plasma Process. Polym.*, vol. 16, no. 7, pp. 1–14, Jul. 2019.
[69] Y.-T. Wang and Y.-T. Yeh, “Effect of Print Angle on Mechanical Properties of FDM 3D Structures Printed with POM Material,” in *Lecture Notes in Mechanical Engineering*, vol. PartF9, 2017, pp. 157–167.
[70] S. Odi-Owei and D. J. Schipper, “Tribological behaviour of unfilled and composite polyoxymethylene,” *Wear*, vol. 148, no. 2, pp. 363–376, Aug. 1991.
[71] R. P. Kusy and J. Q. Whitley, “Degradation of plastic polyoxymethylene brackets and the subsequent release of toxic formaldehyde,” *Am. J. Orthod. Dentofac. Orthop.*, vol. 127, no. 4, pp. 420–427, Apr. 2005.
[72] “Shrinkage Value of Plastics Material & Injection Molding - Chart.” [Online]. Available: https://omnexus.specialchem.com/polymer-properties/properties/shrinkage. [Accessed: 14-Aug-2020].
[73] S. R. Rajpurohit and H. K. Dave, “Effect of process parameters on tensile strength of FDM printed PLA part,” *Rapid Prototyp. J.*, vol. 24, no. 8, pp. 1317–1324, Nov. 2018.
[74] J. M. Chacón, M. A. Caminero, E. García-Plaza, and P. J. Núñez, “Additive manufacturing of PLA structures using fused deposition modelling: Effect of process parameters on mechanical properties and their optimal selection,” *Mater. Des.*, vol. 124, pp. 143–157, 2017.
[75] A. D638-14, “ASTM D638-14: Standard Test Method for Tensile Properties of Plastics1,” *ASTM Int.*, vol. 82, no. C, pp. 1–15, 2016.
[76] C. Wendt *et al.*, “Preliminary Design and Analysis of Tensile Test Samples Developed by Additive Manufacturing,” *Procedia Eng.*, vol. 132, pp. 132–139, 2015.
[77] K. P. Menard, “Dynamic Mechanical Analysis DYNAMICAL MECHANICAL ANALYSIS,” *Encycl. Anal. Chem.*, pp. 1–22, 2017.
[78] American Society for Testing and Materials, “Standard Test Method for Plastics: Dynamic Mechanical Properties: In Flexure (Three-Point Bending),” *ASTM Int.*, vol. D5023, pp. 1–3, 2015.
[79] “Torsion Test.” [Online]. Available: https://www.testresources.net/applications/test-types/torsion-test/. [Accessed: 26-Jul-2020].
[80] American Society for Testing and Materials, “ASTM E1430-13: Standard Test Method for shear Modulus at Room Temperature1,” *Astm*, vol. 87, no. November 2001, pp. 1–6, 1987.
[81] A. K. Sood, R. K. Ohdar, and S. S. Mahapatra, “Parametric appraisal of fused deposition modelling process using the grey Taguchi method,” *Proc. Inst. Mech. Eng. Part B J. Eng. Manuf.*, vol. 224, no. 1, pp. 135–145, Jan. 2010.

[82] S. Wacharawichanant and T. Siripattanasak, “Mechanical and Morphological Properties of Polypropylene/Polyoxymethylene Blends,” *Adv. Chem. Eng. Sci.*, vol. 03, no. 03, pp. 202–205, 2013.
[83] J.-Z. Liang, “Predictions of Storage Modulus of Glass Bead-Filled Low-Density-Polyethylene Composites,” *Mater. Sci. Appl.*, vol. 01, no. 06, pp. 343–349, 2010.
[84] K. S. Boparai and R. Singh, “Thermoplastic Composites for Fused Deposition Modeling Filament: Challenges and Applications,” in *Reference Module in Materials Science and Materials Engineering*, Elsevier, 2018, pp. 1–14.
[85] A. Katunin and A. Gnatowski, “Influence of heating rate on evolution of dynamic properties of polymeric laminates,” *Plast. Rubber Compos.*, vol. 41, no. 6, pp. 233–239, 2012.
[86] TA Instruments, “Measurement of the Glass Transition Temperature Using Dynamic Mechanical Analysis,” *TA Instruments*, vol. I, p. 1997, 1997.
[87] E. Azhikannickal and A. Uhrin, “Dimensional stability of 3D printed parts: Effects of process parameters,” *Ohio J. Sci.*, vol. 119, no. 2, pp. 9–16, 2019.
[88] F. Górski, W. Kuczko, and R. Wichniarek, “INFLUENCE OF PROCESS PARAMETERS ON DIMENSIONAL ACCURACY OF PARTS MANUFACTURED USING FUSED DEPOSITION MODELLING TECHNOLOGY,” *Adv. Sci. Technol. – Res. J.*, vol. 7, no. 19, pp. 27–35, Sep. 2013.
[89] J. Kacmarcik, D. Spahic, K. Varda, E. Porca, and N. Zaimovic-Uzunovic, “An investigation of geometrical accuracy of desktop 3D printers using CMM,” *IOP Conf. Ser. Mater. Sci. Eng.*, vol. 393, no. 1, p. 012085, Aug. 2018.
[90] T. Nancharaiah, D. R. Raju, and V. R. Raju, “An experimental investigation on surface quality and dimensional accuracy of FDM components,” *J. Thermoplast. Compos. Mater.*, vol. 26, no. 5, pp. 680–698, Jun. 2013.
[91] C. K. Basavaraj and M. Vishwas, “Studies on Effect of Fused Deposition Modelling Process Parameters on Ultimate Tensile Strength and Dimensional Accuracy of Nylon,” *IOP Conf. Ser. Mater. Sci. Eng.*, vol. 149, no. 1, p. 012035, Sep. 2016.
[92] Y. Yang, Y. Chen, Y. Wei, and Y. Li, “3D printing of shape memory polymer for functional part fabrication,” *Int. J. Adv. Manuf. Technol.*, vol. 84, no. 9–12, pp. 2079–2095, 2016.
[93] J. R. Wagner, E. M. Mount, and H. F. Giles, “25 - Design of Experiments,” in *Extrusion (Second Edition)*, Second Edi., J. R. Wagner, E. M. Mount, and H. F. Giles, Eds. Oxford: William Andrew Publishing, 2014, pp. 291–308.
[94] M. Islam, B. Boswell, and A. Pramanik, “Dimensional accuracy achievable by three-dimensional printing,” in *IAENG Transactions on Engineering Sciences*, no. April, CRC Press, 2014, pp. 263–268.
[95] K.-E. Aslani, K. Kitsakis, J. D. Kechagias, N. M. Vaxevanidis, and D. E. Manolakos, “On the application of grey Taguchi method for benchmarking the dimensional accuracy of the PLA fused filament fabrication process,” *SN Appl. Sci.*, vol. 2, no. 6, 2020.
[96] H. Staudinger and N. Laureate, “18.1 Overview,” 2020, pp. 473–480.
[97] G. Kumar, N. R. Neelakantan, and N. Subramanian, “Polyacetal and thermoplastic polyurethane elastomer toughened polyacetal: crystallinity and fracture mechanics,” *J. Mater. Sci.*, vol. 30, no. 6, pp. 1480–1486, 1995.

Appendix A

Matlab code for drawing two problems caused by 2.5D contours

A.1 Staircase Effect

```
clear all
clc
X = linspace(0,2,5);     %set range
Y = X;     %draw the actual outline
Z = X;     %draw the ideal outline

figure
plot(Z,'--')
hold on
stairs(Y)
```

A.2 Containment Problem

```
clear all
clc
X = linspace(0,4,10);     %set range
Y = X.*(X>=0&X<2)+1.15*X.*(X>=2&X<4);     %draw different actual outlines
Z = X;     %draw the ideal outline

figure
plot(Z,'--')
hold on
stairs(Y)
```

Appendix B
Dual Nozzle Extrusion Setup

Ultimaker 3 provides the capacity to prepare dual material prints or printing with two colors. This appendix introduces the basic settings and calibrations of dual-nozzle extrusion.

1. **Printcore Installation**
   In the Material/Printcore setting, choose to replace the printcore, open the print head fan bracket, and insert the printcore to complete the installation.

2. **Materials Loading**
   In the Material/Printcore setting, choose to load materials, place the spool of filament on the spool holder, and insert the end of the filament into the feeder. Wait for the nozzle to heat until the material is extruded from the print head.

3. **Bed Leveling**
   In the System/Build plate setting, choose manual leveling according to the system prompts, make rough leveling, and then make fine-tuning so that the frictional force of the nozzle and the three points is the same (calibration card required to determine the friction).

4. **Z offset Calibration**
   In the System/Maintenance setting, select Z offset calibration, place the calibration card between the second nozzle and the build plate, then rotate the button to lower the nozzle height until you feel slight friction when moving the card.

5. XY offset Calibration

In the System/Maintenance setting, select XY offset, the printer will print a set of grid patterns, wait for the printing to complete, compare the patterns with the XY calibration paper, and determine the values of the X and Y offset.